

# Determination of thermodynamics and kinetics of RNA reactions by force

Ignacio Tinoco Jr.<sup>1\*</sup>, Pan T. X. Li<sup>1</sup> and Carlos Bustamante<sup>1,2</sup>

<sup>1</sup> Department of Chemistry, University of California, Berkeley, CA, USA

<sup>2</sup> Departments of Physics, and Molecular and Cell Biology, Howard Hughes Medical Institute, University of California, Berkeley, CA, USA

---

**Abstract.** Single-molecule methods have made it possible to apply force to an individual RNA molecule. Two beads are attached to the RNA; one is on a micropipette, the other is in a laser trap. The force on the RNA and the distance between the beads are measured. Force can change the equilibrium and the rate of any reaction in which the product has a different extension from the reactant. This review describes use of laser tweezers to measure thermodynamics and kinetics of unfolding/refolding RNA. For a reversible reaction the work directly provides the free energy; for irreversible reactions the free energy is obtained from the distribution of work values. The rate constants for the folding and unfolding reactions can be measured by several methods. The effect of pulling rate on the distribution of force-unfolding values leads to rate constants for unfolding. Hopping of the RNA between folded and unfolded states at constant force provides both unfolding and folding rates. Force-jumps and force-drops, similar to the temperature jump method, provide direct measurement of reaction rates over a wide range of forces. The advantages of applying force and using single-molecule methods are discussed. These methods, for example, allow reactions to be studied in non-denaturing solvents at physiological temperatures; they also simplify analysis of kinetic mechanisms because only one intermediate at a time is present. Unfolding of RNA in biological cells by helicases, or ribosomes, has similarities to unfolding by force.

## 1. Introduction 326

## 2. Instrumentation 328

- 2.1 Instruments to study mechanical properties of RNA 328
  - 2.1.1 AFM 328
  - 2.1.2 Magnetic tweezers 328
  - 2.1.3 Optical tweezers 330
- 2.2 Optical trap instrumentation 330
- 2.3 Calibrations 332
  - 2.3.1 Calibration of trap stiffness 332
  - 2.3.2 Calibration of force 333
  - 2.3.3 Calibration of distance 334
- 2.4 Types of experiments 334
  - 2.4.1 Force-ramp 334
  - 2.4.2 Force-clamp or constant-force experiments 335

\* Author for correspondence: Dr I. Tinoco Jr., Department of Chemistry, University of California, Berkeley, CA 94720-1460, USA.

Tel.: 510 642-3038; Fax: 510 643-6232; Email: [intinoco@lbl.gov](mailto:intinoco@lbl.gov)

- 2.4.3 Extension-clamp or constant extension experiments 335
- 2.4.4 Force-jump, Force-drop 336
- 2.4.5 Passive mode 336

### 3. Thermodynamics 336

- 3.1 Reversibility 336
- 3.2 Gibbs free energy 337
  - 3.2.1 Stretching free energy 338
    - 3.2.1.1 Rigid molecules 338
    - 3.2.1.2 Compliant or flexible molecules 339
  - 3.2.2 Free energy of a reversible unfolding transition 339
  - 3.2.3 Free energy of unfolding at zero force 340
  - 3.2.4 Free energy of an irreversible unfolding transition 340
    - 3.2.4.1 Jarzynski's method 341
    - 3.2.4.2 Crooks fluctuation theorem 343

### 4. Kinetics 345

- 4.1 Measuring rate constants 345
  - 4.1.1 Hopping 345
  - 4.1.2 Force-jump, Force-drop 347
  - 4.1.3 Force-ramp 348
  - 4.1.4 Instrumental effects 350
- 4.2 Kinetic mechanisms 351
  - 4.2.1 Free-energy landscapes 351
  - 4.2.2 Kinetics of unfolding 353

### 5. Relating force-measured data to other measurements 354

- 5.1 Thermodynamics 354
- 5.2 Kinetics 357

### 6. Acknowledgements 357

### 7. References 358

## 1. Introduction

The ability to manipulate single molecules and to measure their properties makes it possible to solve problems that could not even be approached earlier. The mechanism of translation is extremely complicated with 61 codons and corresponding transfer RNAs involved in correctly placing 20 amino acids in a polypeptide sequence. Single-molecule methods, in principle, are capable of assessing the effect of each component on the rate of addition of each amino acid, the probability of adding the wrong amino acid, the details of the motion of the messenger RNA (mRNA) and tRNAs through the ribosome, and so forth. Consider the mechanism of minus-one frameshifting during translation of a mRNA (Jacks & Varmus, 1985). A reasonable hypothesis is that pausing of the mRNA leads to increased probability of slippage and frameshifting (Plant *et al.* 2003; Namy *et al.* 2006), but measurements in bulk cannot definitely prove this. However, step-by-step assessment of translation of a single mRNA by a single ribosome would directly correlate the time spent in each step with whether a frameshift occurs. In general, to determine the sequence dependence, or the effect of RNA structure, on the rate of replication, transcription,

translation, exonuclease hydrolysis, and so forth, it is necessary to synchronize the reaction. Such synchronization is not possible in bulk reactions that involve a huge number of molecules. Even if all the enzymes and substrates are identical, and all reactions are started at the same time, the stochastic nature of individual molecular trajectories will quickly destroy the correlation among the molecules. Obviously, a single molecule does not require synchronization. For example, the sequence dependence of the rate of transcription can be measured as a RNA polymerase traverses the DNA (reviewed in Bai *et al.* 2006). The rate constant for transcription at each base pair can be determined (Abbondanzieri *et al.* 2005); this cannot be done in bulk experiments. In fact, although gels can provide single base-pair resolution of transcription pauses, the intensity of each band is a convolution of the probability of pausing at each position in the sequence and the length of the pause, each of which are in themselves stochastic quantities. Thus, while bulk measurements provide information about the dynamics of the *mean* of a population of molecules (chemical kinetics), single-molecule methods make it possible to follow the real-time dynamics of each molecule.

Another valuable capability of single molecule methods is that they provide distributions of properties, whereas bulk measurements give either the average value of molecular properties in a sample, or the sum of the contributions of the properties of each molecule. The proton spectrum of molecules in fast exchange on the NMR timescale is the average of the spectra of the individual species in the sample (Gutowsky & Holm, 1957). Optical spectra, and NMR spectra for molecules in slow exchange, are the sum of the values of properties of all the molecules in the sample. A single molecule has one value for each property at one time. As conformational changes occur, or if a chemical reaction takes place, the time evolution of the properties can be followed. If the data acquisition rate in a single-molecule experiment is fast compared to the kinetics of change, different property values for that molecule will be obtained at different times revealing the distribution of conformations and/or environments of the molecule. The greater the number of single molecules observed, or the greater the number of observations made on a given molecule, the higher the probability of detecting rare species.

RNA molecules must be correctly folded to perform their many biological functions. Study of folding and unfolding pathways by single-molecule manipulation methods reveals possible paths and their relative frequencies (Liphardt *et al.* 2001, 2002; Onoa *et al.* 2003; Collin *et al.* 2005; Li *et al.* 2006). Repeating the process thousands of times can identify paths and intermediates that occur less than 1% of the time. Moreover, paths that lead to misfolded, kinetically trapped species can also be seen. All this information would be very difficult, if not impossible, to obtain by bulk methods.

An advantage unique to single-molecule manipulation methods is the possibility of using force as a controllable variable in experiments, and the ability to apply this force to a molecule without perturbing the other species in the sample. A single RNA molecule can be unfolded at constant temperature in any solvent without perturbing any other molecules in the solution (proteins, ligands, other RNAs). Force can change the equilibrium of any reaction that involves a change of dimension. It can change rates of reactions in which the transition state has a different extension than reactant or product. Force is an additional thermodynamic variable analogous to temperature and pressure; it differs from these traditional intensive variables in that it can be applied to only one molecule in the system. We will describe the methods of applying force to single molecules, and of measuring the thermodynamics and kinetics of RNA reactions using force.

## 2. Instrumentation

Manipulating single biomolecules is technically challenging because of their small size; the contour length of a 1000-nucleotide single-stranded RNA is  $\sim 0.5 \mu\text{m}$  and the force required to change its extension is in the  $10^{-12}$  newton (pN) range. It is particularly difficult to study the unfolding of RNA, if the end-to-end distance of the molecule changes by only a few nanometers. For instance, unfolding a 20-bp RNA hairpin with a loop of four nucleotides increases its extension by less than 20 nm. Three techniques: optical tweezers, atomic force microscopy (AFM), and magnetic tweezers have been used to investigate the mechanical properties of nucleic acid molecules. Detailed descriptions of these techniques have been presented (Sheetz, 1998; Clausen-Schaumann *et al.* 2000; Allison *et al.* 2002; Gosse & Croquette, 2002; Lang & Block, 2002; Smith *et al.* 2003; Neuman & Block, 2004). Here, we will limit our discussion to applications to RNA.

### 2.1 Instruments to study mechanical properties of RNA

#### 2.1.1 AFM

AFM is widely used to image biomolecules on surfaces (Allison *et al.* 2002). In addition, it is a powerful tool to apply mechanical force to various polymers, such as proteins (Rief *et al.* 1997; Fernandez & Li, 2004), polysaccharides (Marszalek *et al.* 2002), cell membranes (Leckband, 1995) and organic polymers (Hugel *et al.* 2002). More recently, AFM has been used to study mechanical properties of double- and single-stranded DNA (Rief *et al.* 1999; Cui *et al.* 2006), double-stranded (ds) RNA (Bonin *et al.* 2002) and to measure the dissociation of short RNA duplexes (Green *et al.* 2004). In these experiments, the molecules of interest are deposited on freshly cleaved mica, which can be moved by a 3D translation stage (Fig. 1*a*). A RNA molecule can be attached to the tip at the end of the AFM cantilever simply by pressing the tip against the surface; a force is then applied to the RNA molecule by moving the stage away from the tip (Bonin *et al.* 2002); forces as high as a few hundred pN can be exerted in this way. The force acting on the molecule can be determined from the bending of the cantilever by measuring the deflection of a laser beam reflected off the cantilever onto a photodetector. The extension of the molecule is determined from the relative positions of the end of the cantilever and the translational stage.

Bonin *et al.* (2002) compared the mechanical properties of dsDNA and dsRNA, including the characteristic overstretching transition at  $\sim 60$  pN (Smith *et al.* 1996). However, attempts to map the secondary structures that can be adopted by single-stranded (ss) RNAs failed in the same study. In these experiments, nucleic acids are attached to mica and to AFM tips through non-specific interactions whose chemical nature is not known. Hence, each single RNA molecule is picked up by the AFM tip at different positions, and thereby each stretching curve has a different contour length. Such uncertainty in the location along the RNA that contacts the cantilever complicates the interpretation of the multiple structures that a large ssRNA can form. In addition, the impossibility of detecting refolding trajectories makes it difficult to distinguish a single molecule from multiple tethers. Given the successful application of AFM to the study of protein folding (Fernandez & Li, 2004), it should be possible in the future to overcome these problems and reveal complicated RNA structures by AFM.

#### 2.1.2 Magnetic tweezers

Magnetic tweezers (Fig. 1*b*) have been used to study the mechanical properties of nucleic acids (Strick *et al.* 1996; Abels *et al.* 2005) and the mechanisms of enzymatic reactions with DNAs as

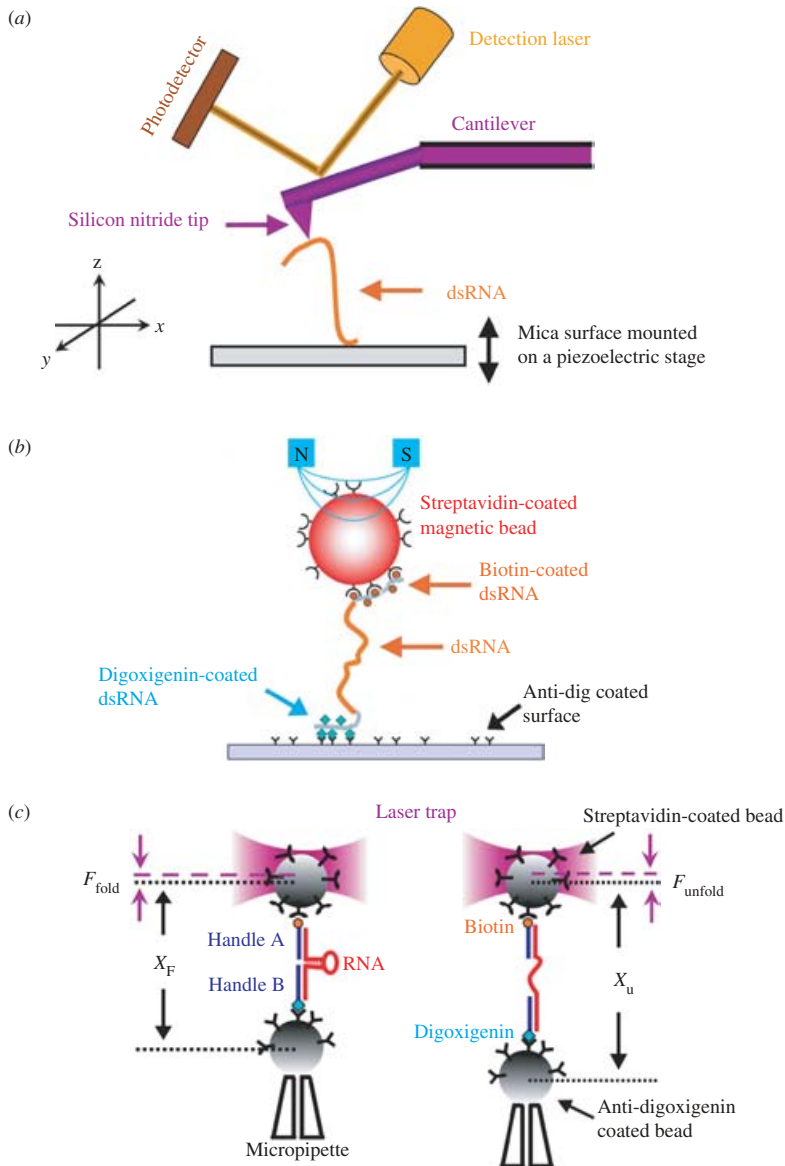


**Fig. 1.** Experiment set-ups for mechanical studies of RNA. (a) Atomic force microscopy (Rief *et al.* 1997). The ‘pulling’ AFM consists of a cantilever, a laser detection system and a moveable surface. The silicon nitride tip of the cantilever picks up RNA molecules by ‘tapping’ on the surface. The position of the cantilever is monitored by the deflection of a detecting laser. RNA samples are placed on a mica surface mounted on a 3D translational stage. Moving the mica in the  $x$  and  $y$  direction allows scanning the surface to find RNA molecules. Then the mica is moved in the  $z$  direction to exert force on the molecule. (b) Magnetic tweezers (Strick *et al.* 1996). Two short pieces of dsRNA, labeled either with digoxigenins or biotins, are ligated to a long dsRNA (Abels *et al.* 2005). The RNA is deposited on a surface coated with anti-digoxigenin antibody. The other end of the molecule is tethered to a magnetic bead coated with streptavidin. By applying a magnetic field, the bead and therefore the RNA can be pulled. (c) Optical tweezers (Smith *et al.* 2003). The RNA is tethered to a pair of beads coated either with streptavidin or anti-digoxigenin antibody (Liphardt *et al.* 2001). The former bead is held in a force-measuring optical trap, shown in purple. The other bead is sucked on the tip of a micropipette by applying vacuum. Position of the micropipette is controlled by a piezo-electric stage. By moving the stage, the RNA is extended and tension is generated.

substrates (Crisona *et al.* 2000; Revyakin *et al.* 2003; Dessinges *et al.* 2004; Gore *et al.* 2006). In a recent study, Abels *et al.* (2005) ligated a long dsRNA (4.2 kb or 8.3 kb) with two 0.4 kb pieces of dsRNA, each of which was labeled by multiple digoxigenins or biotins. The construct was tethered between a streptavidin-coated magnetic bead and anti-digoxigenin antibody-coated surface. By varying the magnetic field, forces of up to 10 pN were generated on the RNA. This study determined the persistence length for dsRNA to be  $\sim 64$  nm, slightly higher than that of dsDNA ( $\sim 50$  nm) (Bustamante *et al.* 1994; Smith *et al.* 1996; Baumann *et al.* 2000). However, the rather low spatial and time resolution ( $\sim 30$  nm and  $\sim 1$  s averaging time) of this method (Gosse & Croquette, 2002) limits the application of this technique in studying RNA folding/unfolding.

### 2.1.3 Optical tweezers

Optical tweezers are the current method of choice for studying RNA folding (Liphardt *et al.* 2001, 2002; Onoa *et al.* 2003; Collin *et al.* 2005; Dumont *et al.* 2006; Li *et al.* 2006). In these experiments, the RNA molecule of interest, flanked by two 'molecular handles' made up of 500 bp dsDNA/RNA hybrids, is tethered between two micron-size beads through affinity interactions (Fig. 1*c*). One of the beads is held in an optical trap while the other is held on a micropipette mounted on a piezoelectric flexure stage. Force is applied to the RNA by moving the micropipette relative to the optical trap; its magnitude is determined either by the displacement of the bead from the center of the trap, or by changes in the light momentum when the bead moves (Smith *et al.* 2003). The relative positions of the two beads determine the extension of the molecule. Optical tweezers can generate forces up to 100 pN with 0.1 pN precision (Smith *et al.* 2003), while most RNA structures unfold in the range of 10–20 pN. An important quantity in single-molecule manipulation is the loading or the unloading rate, the product of the stiffness of the trap and the rate of pulling or relaxation of the molecule, respectively. Typical loading/unloading rates accessible with optical tweezers are in the range of 0.1 and 100 pN/s. Changes in the extension of the molecule between 2 nm and 200 nm have been measured (Onoa *et al.* 2003; Dumont *et al.* 2006). It is possible to observe the reversible folding of a small hairpin with only 7 bp and a tetraloop (P. Li, unpublished data). The elastic property of unstructured ssRNAs, such as poly U, can also be characterized using optical tweezers (Seol *et al.* 2004). Recent additions to optical tweezers instrumentation include temperature control (Williams *et al.* 2001; Mao *et al.* 2005) and a single-molecule fluorescence module (Lang *et al.* 2004; Brau *et al.* 2006). In the following sections, we will discuss the instrumentation and the application of optical tweezers to RNA folding.

## 2.2 Optical trap instrumentation

When a laser beam is focused to a diffraction-limited spot through a high-numerical aperture objective, particles with high refractive indexes are attracted to the most intense part of the beam and held at the focal point (Ashkin *et al.* 1986; Ashkin, 1998). The focused beam creates a nearly harmonic potential so that the force acting on a bead is proportional to the displacement of the bead (for small displacements) from the center of the beam. Lang *et al.* (2002) presented an extensive review on the theory, design and applications of optical traps. More recent reviews have been compiled in *Methods in Enzymology*, Biophotonics, G. Marriott, I. Parker, Eds. Volume 361 (2003). Here we will focus on the dual-beam optical tweezers (Smith *et al.* 2003) that has been used in most of the mechanical folding/unfolding RNA studies.

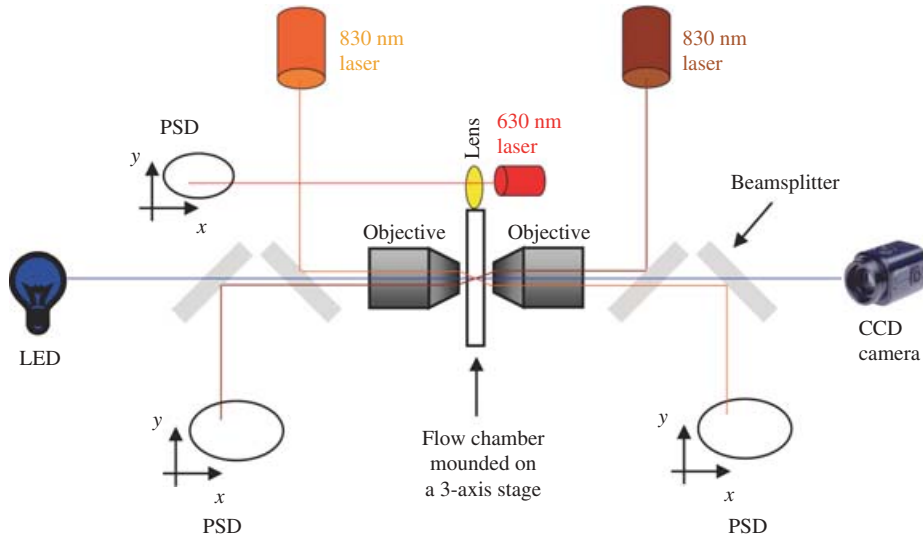


**Fig. 2.** Basic design of a dual-beam optical trap (Smith *et al.* 2003). The reaction occurs in a flow chamber, which is placed between two high numerical aperture objectives and mounted on a piezo-electric stage. Two co-aligned laser beams, generated by a pair of 830 nm lasers (orange and coffee), enter the back of the objectives and are focused in a spot in the flow chamber to create an optical trap. After passing the trap, the beams enter the other objective and become parallel. These rays are then redirected to a pair of photo-sensitive detectors (PSD), which measure the total intensity and positions of the beams. An LED is used to illuminate the chamber and image the focal plane on a CCD camera. To detect the position of the chamber, a light-lever system is used. This system consists of a low power fiber-coupled 630 nm laser, a PSD and a lens with focal length of 1.45 mm mounted on the flow chamber. The lens directs the laser beam on to the PSD. Therefore, the movement of the chamber is monitored by the PSD.

A dual-beam optical trap is created by converging two counter-propagating laser beams to a common focus (Smith *et al.* 2003). In the Berkeley instrument (Fig. 2), the beams generated by two 200 mW, 830 nm diode lasers are focused by a pair of high numerical aperture objective lenses. After passing the focus, each beam comes out of the second objective as a parallel ray and is directed to position-sensitive detectors (PSDs). Each dual-axis detector measures the  $x$  and  $y$  position as well as the intensity of the centroid of the beam exiting from the objective. The laser light enters the objectives as a narrow collimated beam such that nearly all light is collected by the opposite objectives; this arrangement make it possible to measure the light momentum flux of each beam passing through the trapped bead (Smith *et al.* 2003). A force applied to the bead displaces it from the center of the trap and produces a proportional displacement in the beams' centroids on the photodetectors; the magnitude of the force is simply equal to the change of momentum of the light.

Changes in the extension of the molecule are determined by the relative positions of the trapped bead and the bead on the micropipette. The displacement of the trapped bead from the center of the trap,  $\Delta X_{\text{trap}}$ , can be calculated from the force  $F$ , and the spring constant,  $\kappa$ , of the trap ( $\Delta X_{\text{trap}} = F/\kappa$ , calibration of  $\kappa$  is discussed later). The micropipette is fixed relative to the flow chamber, which in turn is firmly mounted on a piezoelectric flexure stage. Hence, the movement of the micropipette is determined by the displacement of the flow chamber by the piezoelectric stage. The position of the flow chamber is measured by a 'light-lever' device (Smith *et al.* 1996). A small lens mounted on the flow chamber collimates and directs a laser beam

(635 nm, 10 mW) on to a third PSD. The movement of the flow chamber is amplified on the PSD by the ratio of the distance to the PSD ( $>500$  mm) to the focal length of the lens (1.45 mm), yielding a distance resolution of  $\sim 1.5$  nm. Alternatively, a capacitive sensor that measures the position of the stage with a resolution of 1 nm, and that is less sensitive to low frequency vibrations by air currents has been used. Combining the position information of the two beads, molecular steps as small as 2 nm can be resolved (Dumont *et al.* 2006). Recent advancement in the instrumentation even pushes the spatial limitation further: Block and colleagues (Abbondanzieri *et al.* 2005), have recently resolved discrete steps of  $3.7 \text{ \AA}$  of RNA polymerase moving along a DNA template.

In addition to the force and extension measurements, video microscopy is used to visualize the experiment. Visible light (from an LED) passes through the two objectives to image the laser focal plane onto a CCD camera with  $60\times$  magnification (Fig. 2). The video images, which are updated at 10–20 Hz, make it possible to visualize the position of trap and the movement of flow chamber, as well as the manipulation of the molecule with the beads.

The RNA molecule is tethered between two beads. Hence, the extension of the molecule can be calculated by subtracting the radii of the two beads from the distance between the centroids of the beads. This method works well with long molecules, such as the  $\sim 48 \text{ kb } \lambda$  DNA (Smith *et al.* 1996). However, the RNAs in our studies ( $\sim 1.1 \text{ kb}$  handles + 20–400 nt ssRNA) are  $< 0.5 \text{ }\mu\text{m}$  in length, i.e. much smaller than the diameter of the beads (2 or  $3 \text{ }\mu\text{m}$ ). The resolution of the camera is  $\sim 10 \text{ nm}$ ; determination of the centroids of the beads has a root-mean-square (rms) uncertainty of 10–15 nm; and the uncertainty in the measurement of bead radius is even higher; hence, at present, the absolute extension of a RNA molecule cannot be determined accurately by our instrument. However, changes in molecular extension are the relevant quantities in RNA folding studies, and these can be measured with nm precision.

### 2.3 Calibrations

Obtaining reliable and reproducible data from optical traps requires careful calibration of the instrument. Many calibration methods have been developed; here we will present the approaches used routinely to calibrate the trap stiffness,  $\kappa$  (pN·nm), the force,  $F$  (pN), and the distance,  $X$  (nm) in our instrument. The trap stiffness, the force and the displacement of the trapped bead from the center of the trap are related by:

$$\kappa = F / \Delta X_{\text{trap}}, \quad (2.1)$$

Usually, the displacement,  $\Delta X_{\text{trap}}$ , is determined from the measured force and calibrated trap stiffness. The  $\Delta X_{\text{trap}}$  is used to determine the changes in extension.

#### 2.3.1 Calibration of trap stiffness

The stiffness of the trap can be calibrated in several ways: (1) drag force, (2) power spectrum and (3) tethered-molecule method.

(1) The drag-force method is based on Stokes' law that relates the drag force experienced by a bead moving relative to a fluid, to its radius ( $r$ ), the viscosity of the fluid ( $\eta$ ) and its velocity ( $v$ ). The Stokes drag coefficient of a bead is  $\gamma = 6\pi\eta r$ . To obtain the data, the flow chamber is moved back and forth by  $\sim 100 \text{ }\mu\text{m}$  at different velocities,  $v$ , and the displacement of the

trapped bead from the center of the trap,  $\Delta X_{\text{trap}}$ , is determined by PSDs or video images (Smith *et al.* 2003). The force on the bead is calculated from Stokes' law, i.e.  $F = \gamma v$ . From these two independently measured quantities ( $v$ ,  $\Delta X_{\text{trap}}$ ) the trap stiffness is obtained.

(2) The power-spectrum method measures the trap stiffness from the power spectrum of the bead fluctuations in the trap (reviewed in Svoboda & Block, 1994; Gittes & Schmidt, 1998). The power spectrum describes the frequency dependence of the mean square displacement of the bead in the trap. It is usually obtained from the Fourier transform of the time-dependent random displacements of the bead. The power spectrum has a Lorentzian shape dependence on frequency,  $\omega$ , being proportional to  $(\omega_c^2 + \omega^2)^{-1}$ , where  $\omega_c$  is the angular corner frequency. As the frequency increases, the magnitude of the power spectrum decreases; the corner frequency is defined as the frequency at which the amplitude of the mean quadratic displacement is at half maximum. Thus, the corner frequency can be obtained by fitting the power spectrum to a Lorentzian.

The trap stiffness,  $\kappa$ , is obtained from the measured corner frequency and the Stokes drag coefficient,  $\gamma$ , of the bead.

$$\kappa = \omega_c \gamma, \quad (2.2)$$

The corner frequency characterizes how fast a trapped bead can move in a viscous medium. A 1  $\mu\text{m}$  radius bead immersed in water, in a laser trap of stiffness 0.1 pN $\cdot$ nm has a corner frequency of  $\sim 5$  kHz. This frequency places an upper limit on the kinetic processes that can be measured.

(3) The tethered-molecule method involves stretching a molecule, such as  $\lambda$  DNA, attached to a trapped bead from 1 to 70 pN. The force in the trap is measured independently (see below);  $\Delta X_{\text{trap}}$  is determined by recording the centroid of the bead. The value of  $\kappa$  is the ratio of the two [Eq. (1)]. Because of the resolution of the centroid determination ( $\sim 10$  nm), a force range of at least 50 pN is required to determine  $\kappa$ .

If the laser beams forming the dual-beam trap are well aligned, all three calibrations should yield very similar values of  $\kappa$  despite the different assumptions and variables measured in each method. The trap stiffness varies with the laser output power; in most published work, the value of  $\kappa$  ranges from 0.05 to 1.2 pN $\cdot$ nm. In our experiments,  $\kappa$  is usually  $\sim 0.1$  pN $\cdot$ nm.

### 2.3.2 Calibration of force

The force exerted on the trapped bead can be determined by several methods (Svoboda & Block, 1994; Gross, 2003; Smith *et al.* 2003). The force determination for the dual-beam trap is based on the conservation of light momentum. A force applied to the bead moves the bead away from the center of the trap and deflects the laser beam. The deflection of the beam corresponds to a rate of change of momentum of the light. Because linear momentum is a conserved quantity in nature, this rate of change of momentum is equal and opposite in sign to the force acting on the bead, i.e. force on the bead =  $-d(\text{light momentum})/dt$ . The deflection of the beams – the change in light momentum – is measured by position-sensitive detectors. The force is thus measured independent of the laser power, bead size, solvent viscosity, etc. A 'force calibration factor' is needed to convert the measured momentum flux of the light to force; a detailed procedure has been described by Smith *et al.* (2003). For a trap with fixed optical and electrical components, the force calibration factor does not vary. This feature allows reliable force measurement over many

experiments and over long periods of time. As a routine test of the force calibration we stretch molecules with known force-extension curves. A good standard is a long dsDNA ( $> 12$  kb) such as  $\lambda$  DNA. In 100 mM NaCl, its force-extension curve displays a characteristic overstretching plateau at  $\sim 65$  pN (Smith *et al.* 1996). RNA hairpins that unfold near 20 pN and with a narrow distribution of unfolding forces ( $< 0.5$  pN) are also useful for this purpose.

### 2.3.3 Calibration of distance

Changes in the extension of the molecule are determined by both the motion of the trapped bead and the movement of the bead on the micropipette. The former is calculated by the ratio of force and trap stiffness; the latter is measured either by the light-lever system or the capacitive sensor. The ranges of the light-lever and the capacitive sensor are  $\sim 100$  nm. To convert their electrical signals to distances, comparison to a known distance must be made. A linear variable differential transformer (LVDT) is attached to the piezoelectric stage that drives the micropipette. The LVDT has a range of 10 mm and a resolution  $\sim 15$  nm. We first calibrate the LVDT signal against a known length standard, such as a caliper. Then both the light-lever and the capacitive sensor are calibrated against the LVDT. A change in distance of  $> 1$  nm can be detected. The pixel distance in the video images can also be calibrated by correlating the centroid position of the bead on the micropipette with the motion of the piezoelectric stage.

## 2.4 Types of experiments

Force can be applied to a molecule in different ways; accordingly several different types of optical tweezers experiments have been developed. These are: force-ramp (pulling), force-clamp (constant force, hopping), force-jump, extension-clamp and passive-mode experiments. We will briefly discuss the implementation, and the parameters measured in each.

### 2.4.1 Force-ramp

In force-ramp experiments, the molecule is repeatedly stretched and relaxed. A force-ramp is usually the first experiment after a tether is found between the two beads. The resulting force-extension curve is indicative of whether the tether is a single molecule or several molecules. For instance, the force-extension curve of a single molecule follows the worm-like-chain (WLC) model (Fig. 3); but that of multiple tethers usually appears like a Hookian spring, i.e. force increases linearly with extension. In a typical experiment, the piezoelectric stage is moved at constant velocity (nm/s). Under these conditions, the tension on the RNA molecule changes approximately linearly with time between 3–20 pN, and thus, the loading rate ( $dF/dt$  in units of pN/s) is approximately constant. When a structural transition occurs, there is a sudden change in force and extension. For instance, when a hairpin unfolds, the extension of the molecule increases abruptly and the trapped bead quickly moves back towards the center of the trap. Hence, on the force-extension curve, the unfolding is characterized by a ‘rip’ with an increase in extension ( $\Delta X$ ) and a decrease in force ( $\Delta F$ ) (Liphardt *et al.* 2001). Similarly, the refolding of a RNA is usually indicated by a ‘zip’, a sudden decrease in extension and increase in force. The force-ramp experiment is simple to implement and is a powerful way to profile the molecular transitions. For reversible transitions the Gibbs free energy is obtained from the work done on the molecule, i.e. the integral of force over distance.

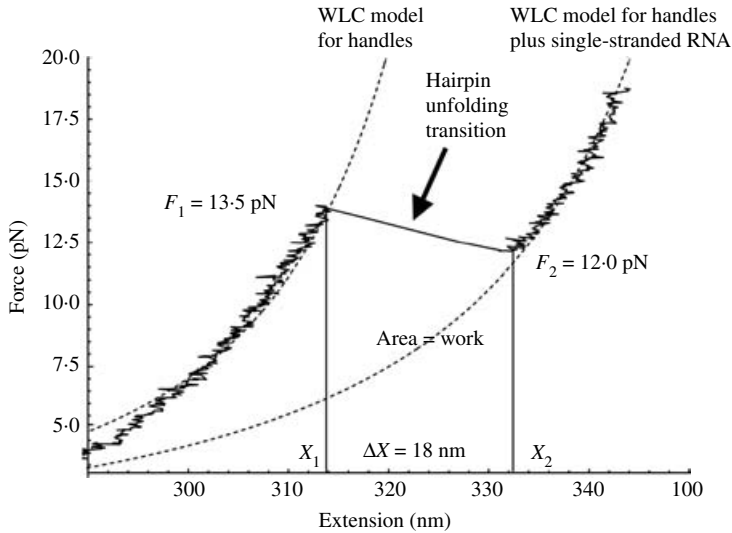


**Fig. 3.** A force-extension curve for a RNA hairpin. A single RNA hairpin flanked by  $\sim 500$  bp DNA/RNA handles was pulled at a constant rate of 1 pN/s. First, the force increases monotonically as the handles are stretched. The force-extension relationship can be modeled (left dashed curve) using a WLC interpolation formula (Bustamante *et al.* 1994) with a persistence length of 10 nm and a contour length of 0.34 nm/bp (Liphardt *et al.* 2001). A rip at 13.5 pN indicates that the hairpin unfolded – the base pairs broke – in a single step with an increase in extension of 18 nm. The breaking of the base pairs decreases the force and produces a rip with a slope approximately equal to the spring constant of the trap ( $\kappa$ ). After the rip, both handles and the unfolded RNA are stretched. The force-extension of this region also fits the WLC model (right dashed curve) with addition of the effect of the single-stranded region. The mechanical work to unfold the hairpin is the area under the rip. Under reversible condition, the mechanical work equals the unfolding/folding free-energy change of the hairpin (Liphardt *et al.* 2001).

#### 2.4.2 Force-clamp or constant-force experiments

In some experiments it is advantageous to hold the force on the molecules constant over the time the experiment lasts. In these conditions, folding/unfolding reactions manifest as changes in extension. Such experiments are particularly useful for RNA hairpins that display bi-stability (hopping) (Liphardt *et al.* 2001). By holding the force constant at a given value, rate coefficients can be obtained directly from the lifetimes of the folded and unfolded states, and free energies can be calculated from the ratio of the kinetic coefficients. By varying the force, it is possible to map the force dependence of the kinetic and thermodynamic parameters of the reaction. Force feedback mechanisms are required to maintain relatively constant force. A proportional integral derivative (PID) algorithm is employed and fine-tuned to adjust the micropipette position to compensate the force changes. Under force-clamp conditions, the extension of the molecule can be continuously monitored over a period of up to 2 h. With an averaging time window of 20 ms, the standard deviation of the force can be controlled to values as small as 0.3 pN. The force-clamp mode is most applicable to RNAs that unfold/refold with lifetimes in the range of 0.1–10 s. For these RNAs, the force range in which the molecule hops is narrow (1–2 pN).

#### 2.4.3 Extension-clamp or constant extension experiments

The extension clamp method is analogous to force-clamp, but now the distance is held fixed and the force is allowed to vary. When the extension of a molecule is held constant, a change in force

is the signature of a structural transition. Similar to the force-clamp method, the position of the micropipette is adjusted to maintain a constant extension by a PID algorithm.

#### 2.4.4 Force-jump, force-drop

In force-jump experiments, the force is kept constant employing the same force feedback mechanism as in force-clamp experiments. However, unlike the force-clamp mode, unfolding and refolding rate constants are measured independently. In a typical experiment, force is first quickly stepped to a set value to monitor the unfolding. After the rip occurs (and the lifetime is noted) the force is increased to ensure complete unfolding; then the force is rapidly dropped to a second value to follow the refolding transition (Li *et al.* 2006). The force-jump method is an extension of the force-clamp experiments, and it is not limited by the reversibility of the reaction. We have used force-jump experiments to unfold complicated RNA structures in a stepwise fashion and to measure the rate constants of individual steps (P. Li *et al.* unpublished observations).

#### 2.4.5 Passive mode

In passive mode, a tethered molecule under tension is not constrained (no feedback is applied) while force and extension are recorded (M. Manosas *et al.* unpublished observations; J.-D. Wen *et al.* unpublished observations). The pipette is standing still; and the distance from the pipette bead to the center of the trap is fixed. Hopping of RNA hairpins between the folded and the unfolded state can be followed in passive mode if the tension applied to the molecule is such that the (force dependent) equilibrium constant for the unfolded transition is not too far from unity, so that both, folding and unfolding rates are of comparable magnitude. In the folded state, the end-to-end distance of the hairpin is short; the trapped bead is pulled away from the center of the trap so that force is relatively high. In the unfolded state, the end-to-end distance of the ssRNA is long; the trapped bead is closer to the center of the trap and the force is low. Therefore, when the RNA transits between folded and unfolded states, both force and extension change. Rate constants and folding free energy can be obtained from such experiments (J.-D. Wen *et al.* unpublished observations).

### 3. Thermodynamics

#### 3.1 Reversibility

We will describe the equilibrium properties that can be measured by applying force to single molecules. The thermodynamic variables measured are force (an intensive variable) and extension or end-to-end distance (an extensive variable). To make the discussion specific, let us start by analyzing a pulling curve resulting from a force-ramp experiment on a RNA hairpin (Fig. 3). The RNA is the TAR hairpin with a 22 bp stem and a 6-nucleotide loop; it is in a buffer of 250 mM NaCl, and the measurements were done at room temperature (Li *et al.* 2006). The RNA is connected to two beads by double-stranded handles (Fig. 1*c*), and the distance between the pipette bead and the laser trap is increased linearly with time. Force and extension are measured as described in the Experimental section. Because of the nearly linear nature of the force extension curve in the unfolding/refolding force region, the force loading rate ( $dF/dt$ ) is approximately constant.

The force-extension curve displays three regimes. The first region corresponds to the stretching of the double-stranded handles. In the second region, there is an abrupt increase in extension as the RNA base pairs break and the RNA unfolds. Finally the double-stranded handles plus the RNA single strand stretch. In order to learn about RNA unfolding, we first need to consider the effect of the handles.

We assume that the pulling curve in Fig. 3 is reversible; that means the loading rate is slow compared to the kinetics of the molecular processes. It is possible to find a criterion to insure that a process can be performed reversibly or quasi-statically. Assume that the RNA molecule is being stretched at a constant rate  $v$ , so that both position and force are allowed to fluctuate, neither one being held fixed. Then, a process occurs reversibly or quasi-statically if throughout the extension (Keller *et al.* 2003):

$$\kappa v \tau < \Delta F_{\text{rms}} = \sqrt{k_B T \kappa}, \quad (3.1)$$

or

$$\sqrt{\frac{\kappa}{k_B T}} v < \frac{1}{\tau}$$

where  $\Delta F_{\text{rms}}$  is the root-mean-square thermal fluctuations of the force on the bead in the trap,  $\kappa$  is the stiffness of the optical trap,  $k_B$  is the Boltzmann constant, and  $\tau$  is the molecular relaxation time for the process of interest (unfolding in this case), the time scale relevant to for the return of the system to equilibrium after a newly imposed end-to-end extension.

An experimental test of reversibility is whether the curve is the same when the force is increased or decreased, i.e. whether there is hysteresis. The relaxation times involved in the stretching of the handles are fast compared to the loading rates used during unfolding studies ( $< 100$  pN/s); thus, stretching and relaxation of handles show no hysteresis. By contrast, the kinetics of the RNA unfolding transition is often slow, the inequality of Eq. (3.1) may not be fulfilled, and the unfolding transition may not be reversible even at relatively slow loading rates ( $\sim 1$  pN/s). Note that because of drift in the instrument it may be difficult to use loading rates smaller than  $0.1$  pN/s to achieve reversibility. However, free energies can still be obtained for irreversible transitions, and valuable kinetic data can also be determined, as we will describe later.

### 3.2 Gibbs free energy

For a reversible mechanical process, the reversible work ( $dw = FdX$ ) is equal to the Gibbs free-energy change,  $dG[X]$ , at constant temperature,  $T$ , and pressure,  $P$ .

$$dG[X] = -SdT + VdP + FdX, \quad (3.2)$$

The entropy is  $S$ , the volume is  $V$ , the force is  $F$ , and the extension is  $X$ . We use the notation  $G[X]$  to emphasize that the free energy depends on an extensive variable  $X$ . Gibbs originally defined free energy to transform the internal energy, dependent on extensive variables  $S$  and  $V$ , to a more useful function dependent on intensive variables  $T$  and  $P$ , which are the variables usually controlled in the laboratory. Similarly, we apply a Legendre transform,  $G[F] = G[X] - FX$ , to obtain the force representation of free energy with the intensive variable  $F$  replacing the extensive variable  $X$ .

$$dG[F] = -SdT + VdP - XdF, \quad (3.3)$$

**Table 1.** Energy units used in force-extension experiments

Energy unit	pN·nm	$k_B T$ (298 K)	Joule	kJ/mol	kcal/mol
1 pN·nm =	1	0.2430	$1 \times 10^{-21}$	0.6022	0.1439
1 $k_B T$ (298 K) =	4.114	1	$4.114 \times 10^{-21}$	2.478	0.5921
1 Joule =	$1 \times 10^{+21}$	$0.2430 \times 10^{+21}$	1	$0.6022 \times 10^{+21}$	$0.2390 \times 10^{+21}$
1 kJ/mol =	1.661	0.4036	$1.661 \times 10^{-21}$	1	0.2390
1 kcal/mol =	6.949	1.689	$6.948 \times 10^{-21}$	4.184	1

One newton/meter = 1 joule, therefore 1 piconewton ( $10^{-12}$  N) · nanometer ( $10^{-9}$  m) =  $10^{-21}$  J = 1 zeptojoule.

In these equations temperature and pressure apply to the entire system (solvent, buffer, ligands, etc.); force and extension refer only to the one unique molecule. As a result, fluctuations in  $T$  and  $P$  can be considered negligible relative to their average values. However, the thermal fluctuations in  $F$  and  $X$  for a single molecule will in general be of the same order of magnitude as their average values. Therefore, we should be aware that a constant force, for example, means a constant average force and that, fluctuations in the force, and therefore in the free energy, will be significant. Typical standard deviation of force can be controlled within 0.3 pN (Lang *et al.* 2002; Li *et al.* 2006). More recent developments allow even better control of the force (Greenleaf *et al.* 2005). Another difference between the usual thermodynamic variables and  $F$  and  $X$  is that the latter are vectors. The effect of force on the free energy of a molecule depends not only on the point of application, but also on the direction of application.

The most direct units of free energy for mechanical processes are pN·nm. But for comparison with other measurements, and because chemists and physicists prefer different units, we present a conversion table (Table 1).

### 3.2.1 Stretching free energy

The pulling curve in Fig. 3 and nearly all the processes we consider are obtained at constant  $T$ , and  $P$ . The change in free energy can be calculated directly by integrating Eq. (3.4) or Eq. (3.5).

$$G[X_2] - G[X_1] = \int_{X_1}^{X_2} F dX, \quad (3.4)$$

$$G[F_2] - G[F_1] = - \int_{F_1}^{F_2} X dF. \quad (3.5)$$

Or, the definitions of the two free energy representations can be used to relate one representation to the other.

$$G[F_2] - G[F_1] = G[X_2] - G[X_1] - (F_2 X_2 - F_1 X_1). \quad (3.6)$$

#### 3.2.1.1 Rigid molecules

The effect of a force on the free energy of a molecule depends on the elastic properties of that molecule. For a rigid molecule,  $X$  is independent of force. Thus,  $G[X]$  is independent of force

and  $G[F]$  is linearly dependent on force.

$$G[X] - G[X] = 0, \quad (3.7)$$

$$G[F_2] - G[F_1] = -X(F_2 - F_1). \quad (3.8)$$

### 3.2.1.2 Compliant or flexible molecules

In this case, both the  $G[X]$  and  $G[F]$  will depend on force. In particular, for a flexible polymer, equations that only consider entropic contributions to mechanical properties are often useful approximations. The WLC model (Flory, 1969), and the freely-jointed chain model (FJC) (Jernigan & Flory, 1968) are most popular, but other equations are also appropriate (Cocco *et al.* 2003b; Rosa *et al.* 2005; Wiggins *et al.* 2005). The WLC model uses a single molecular parameter, the persistence length, to characterize the force-extension curve for a polymer of given contour length. An interpolation formula (Bustamante *et al.* 1994) has proven very useful:

$$F_{\text{WLC}} = \left[ \frac{\kappa_B T}{P} \right] \left[ \frac{1}{4(1-X/L)^2} + \frac{X}{L} - \frac{1}{4} \right]. \quad (\text{WLC model}) \quad (3.9)$$

The force is  $F$ ,  $T$  is the temperature,  $\kappa_B$  is Boltzmann's constant,  $L$  is the contour length of the polymer,  $X$  is the end-to-end distance – the extension, and  $P$  is the persistence length. The dashed lines in Fig. 3 are Eq. (3.9) fit to the stretching of the handles and ssRNA. A contour length of 0.29 nm per base pair is used for the double strands and 0.59 nm per nucleotide for the ssRNA. The persistence length is an adjustable parameter to best fit the experimental curves. We use  $P=1$  nm for ssRNA and  $P=10$  nm for the double-stranded RNA•DNA handles.

The free energy,  $G[X]$ , of a flexible polymer increases because work must be done on the molecule by the external force as the coil form with its many different conformations is extended into a more linear form, thus reducing the molecule's entropy. The increase in free energy is the integral of the force times the distance.

$$G[X] - G(0) = \kappa_B T \left( \frac{L}{P} \right) \left[ \frac{3(X/L)^2 + 2(X/L)^3}{4(1-(X/L))} \right]. \quad (3.10)$$

Notice that the free energy, an extensive property, is directly proportional to the contour length of the polymer. A single-strand nucleic acid ( $P=1$  nm) with a contour length of 100 nm ( $\sim 170$  nucleotides) when extended to 70% will increase in free energy by  $65 \kappa_B T$  or 161 kJ/mol at 25 °C.

### 3.2.2 Free energy of a reversible unfolding transition

When a RNA unfolds (assumed reversibly) between  $F_1$  and  $F_2$  with a change in extension of  $(X_2 - X_1)$  (see Fig. 3), the work done is equal to the Gibbs free-energy change. It is the area under the transition curve – the rip. As the transition is rapid compared to the data acquisition rate, the transition ‘curve’ is a straight line joining the start and end of the transition. The slope of this rip is approximately equal to the stiffness of the laser trap. The extension representation of the Gibbs free energy (equal to the sum of the area under the rip) is thus

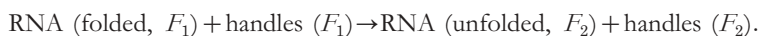
$$\Delta G_{\text{transition}}[X] = \frac{(F_1 + F_2)(X_2 - X_1)}{2}. \quad (3.11)$$

It is the free energy of unfolding the RNA at an initial force  $F_1$  to an unfolded single strand at force  $F_2$ . The force representation of the Gibbs free energy change is the area under the curve projected on the force axis.

$$\Delta G_{\text{transition}}[F] = -\frac{(F_2 - F_1)(X_1 + X_2)}{2}. \quad (3.12)$$

It is straightforward to show that the values of  $\Delta G[X]$  and  $\Delta G[F]$  are consistent with Eq. (3.6). Note that if  $(X_2 - X_1) = 0$ ,  $\Delta G[X] = 0$ , the condition for equilibrium with  $T$ ,  $P$ , and  $X$  constant. If  $(F_2 - F_1) = 0$ ,  $\Delta G[F] = 0$ , the condition for equilibrium with  $T$ ,  $P$ , and  $F$  constant.

The free energies measured above have contributions from the RNA unfolding and from the handles (Liphardt *et al.* 2001). The transition is



We assume that the folded RNA is rigid, so its  $G[X]$  is independent of force. Of course, the handles and the single-stranded, unfolded RNA do depend on force.

$$\Delta G_{\text{transition}}[X] = \Delta G_{\text{RNA}}[X] + \Delta G_{\text{handles}}[X].$$

The  $\Delta G_{\text{handles}}[X]$  is calculated from the WLC model (Bustamante *et al.* 1994). To illustrate the magnitude of the change in free energy of the handles, we choose a 1 kb handle ( $L = 290$  nm) with  $P = 10$ . At 298 K Eq. (3.10) gives  $\Delta G_{\text{handles}}[X] = -20.1$  pN·nm; Eq. (3.11) gives  $\Delta G_{\text{transition}}[X] = (25.5)(18)/2 = 229.5$  pN·nm; thus  $\Delta G_{\text{RNA}}[X] = 249.6$  pN·nm. This free-energy change refers to the unfolding of the RNA to a single strand at  $F_2 = 12.0$  pN.

### 3.2.3 Free energy of unfolding at zero force

In the usual experiments nucleic acids (or proteins) are unfolded by increasing temperature, or by using a denaturing solvent. The free energies at 25 °C or 37 °C are obtained by extrapolating to these temperatures, or by extrapolating to zero denaturant. In force unfolding, the temperature and solvent conditions are chosen, and force is applied to the molecule. To obtain the free-energy change for RNA unfolding at zero force, we must correct for the free-energy change of stretching the RNA single strand from 0 to 12.0 pN. We assume that force only affects the single strand and we use the worm-like chain.

$$\Delta G_{\text{RNA}}^{\circ} \text{ at zero force} = \Delta G_{\text{RNA}}[X] \text{ at } F - \Delta G_{\text{stretch}}[X].$$

The free energy to stretch a ssRNA of 52 nucleotides ( $L = 30.7$  nm,  $P = 1$  nm) to 12.0 pN is  $\Delta G_{\text{stretch}}[X] = 75.8$  pN·nm. The standard free energy of unfolding at 25 °C and zero force is thus  $\Delta G_{\text{RNA}}^{\circ} = 173.8$  pN·nm. We could have obtained the same value of  $\Delta G_{\text{RNA}}^{\circ}$  from  $\Delta G_{\text{RNA}}[F]$  values.

### 3.2.4 Free energy of an irreversible unfolding transition

When the unfolding transition is irreversible – the loading rate is fast compared to the slowest relaxation rate in the molecule, the Gibbs free-energy change is no longer equal to the work done on the molecule; work is dissipated in the process and hysteresis occurs, i.e. the unfolding force-extension curve does not coincide with the refolding curve. In general, because unfolding is a thermally activated process, the force at which it occurs is a stochastic variable and there will be a

distribution of transition forces. As the loading rate increases, the hysteresis increases, the average transition force increases, and the distribution of transition forces widens. Valuable kinetic data can be obtained from irreversible unfolding transitions but, most significantly, because of the microscopic nature of the system, it is possible to recover the reversible work performed in the process, i.e. the free energies of unfolding.

#### 3.2.4.1 Jarzynski's method (Jarzynski, 1997)

The second law of thermodynamics tells us that the work done on a system at constant  $T$  and  $P$  is equal to, or greater than, the Gibbs free-energy increase. The equal sign is correct for a reversible process; for an irreversible process the work done is greater, because some work is dissipated as heat. For a reversible process the mean work is the free-energy change ( $\Delta G[X]$ ); this is the second law.

$$\Delta G = \langle w_{\text{reversible}} \rangle. \quad (\text{Gibbs}) \quad (3.13)$$

The second law, of course, applies to a microscopic (or nanoscopic) system as well as a macroscopic one. However, for a small system, fluctuations in the work done on the system can be as large as the mean value of the work. There is a distribution of work values. In 1997, Christopher Jarzynski showed that the distribution of work values obtained in an irreversible process that takes a system from an initial to a final state can be used to extract the reversible part of the work, i.e. to obtain the free-energy change in that process, according to:

$$\Delta G = -kT \ln \langle e^{-w/kT} \rangle. \quad (\text{Jarzynski}) \quad (3.14)$$

The derivation of Eq. (3.14) requires that the system start in an equilibrium state at temperature  $T$  and a perturbation is applied with a chosen protocol. The perturbation is arbitrary; it can lead to changes in temperature, cause temperature gradients and chemical reactions, etc. The work is measured and the protocol is repeated. In our experiments the perturbation is extension of the molecule with a chosen loading rate. The averaging represented by the brackets is taken, in principle, over an infinite number of repetitions. This result recalls the definition of a reversible process as quasi-static, i.e. one that takes an infinite time. Jarzynski's result is consistent with the second law, because for a reversible process all the work values are equal to  $w_{\text{reversible}}$  (except for experimental uncertainty), and Eq. (3.14) reduces to Eq. (3.13).

One can show (Ritort *et al.* 2002) that the number of repetitions that must be done to obtain a good estimate ( $\pm 1$  kT) of  $\Delta G$  is proportional to the exponential of the mean dissipated work.

$$\text{Number of experiments} \propto e^{\langle w \rangle - \Delta G} / kT, \quad (3.15)$$

Thus, although Jarzynski's equation is valid in principle for systems of all dimensions and for processes involving arbitrary large dissipations, it is only practical for processes with mean dissipated work of  $< 9$  kT ( $\sim 8000$  repetitions) and it quickly loses utility for larger amounts of dissipated work.

In a distribution of work values, Eq. (3.14) weights the smaller values much more than the larger values. For example the mean of 2 kT and 6 kT is 4 kT [Eq. (3.13)], but the exponential weighted mean from Eq. (3.14) is 2.7 kT. Because the average work done on the system is subject to fluctuations from one trajectory to the next, every once in a while, some of these trajectories will even have zero or negative values of the dissipated work. This is the case when the surroundings, i.e. the thermal bath around the molecule does much of the work. Because of

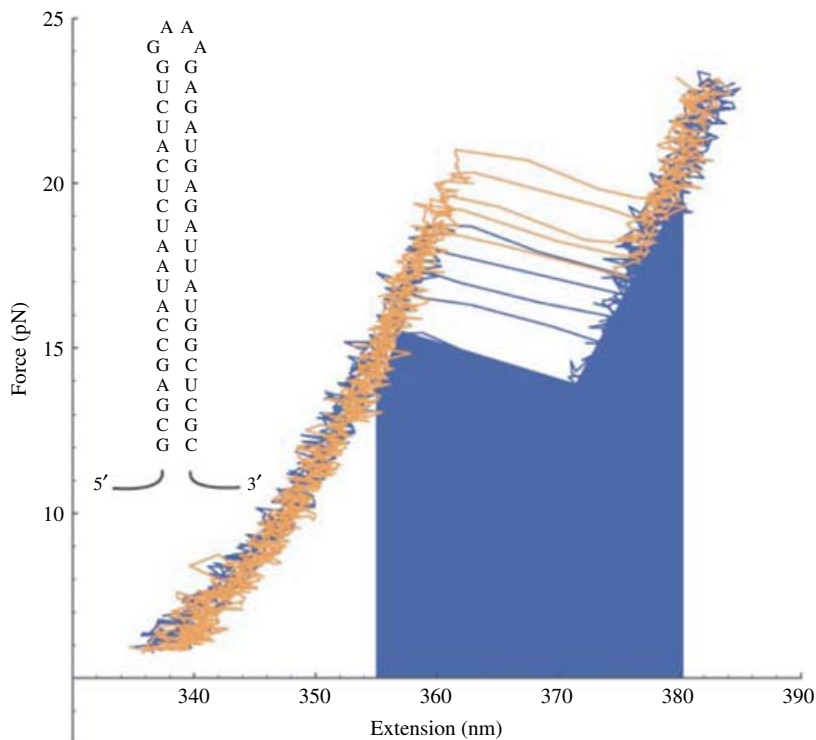


**Fig. 4.** Force-extension curves of irreversible unfolding/refolding. Five cycles of pulling (orange) and relaxation (blue) curves of a hairpin (inset) at a loading rate of 7.5 pN/s show stochastic nature of the unfolding/refolding process (adapted from Collin *et al.* 2005). The hysteresis between the unfolding and refolding indicates the irreversibility. The mechanical work to stretch or relax the RNA plus handles from 355 nm to 380 nm was determined by integrating the area under each trajectory during pulling and relaxation. The area under the lowest refolding curve is shown in blue. The measured mechanical work values were analyzed using Jarzynski's equality and Crooks fluctuation theorem (Collin *et al.* 2005).

the negative exponential averaging involved in Jarzynski's equation, those rare trajectories will be weighted significantly more heavily than the frequent trajectories associated with positive dissipated work. That is, Jarzynski gives the largest weight to trajectories for which thermal fluctuations occur that convert the largest amounts of heat from the environment into useful work on the system. As the mean dissipated work increases, the probability of a trajectory with zero dissipated work decreases exponentially, and the number of experiments that must be done to include those trajectories in the statistics increases exponentially as seen in Eq. (3.15). Once again, in principle (but not in practice) Jarzynski's equation applies to any process no matter how far away from equilibrium and regardless of its size. Because Jarzynski's equation is so novel and counter intuitive, several useful papers have appeared that critique and extend the result (Crooks, 1999; Hummer & Szabo, 2001).

Figure 4 shows five unfolding curves and five refolding curves for a RNA hairpin (Collin *et al.* 2005); the RNA was repeatedly unfolded and refolded at a constant loading rate of 7.5 pN/s. Clearly the process is irreversible; there is hysteresis and a distribution of transition forces. To obtain a free energy from a set of force-extension curves such as these, we measure the work done many times between two chosen extensions and apply Eq. (3.14). Figure 4 shows the refolding work (blue area) obtained as the extension decreases from 380 nm to 355 nm for the

transition that occurs at the lowest force. We measure the work done between the same two extensions for many unfolding trajectories ( $w$  is positive), and many refolding trajectories ( $w$  is negative).

For the data shown in Fig. 4 the mean work done ( $w$ ) in unfolding the RNA and handles between the chosen extensions is  $113.8 \text{ pN}\cdot\text{nm}$ ; the mean work recovered ( $-w$ ) when the RNA and handles refold is  $106.6 \text{ pN}\cdot\text{nm}$ . Applying Jarzynski's equation [Eq. (3.14)] to 380 trajectories of four molecules, we obtain  $109.7 \text{ kT}$  for unfolding and  $110.9 \text{ kT}$  for refolding. These are the Jarzynski estimates for the free-energy change for each process. The average dissipated work is  $\sim 4 \text{ kT}$ , so we expect that about 55 trajectories should be sufficient to obtain a value within  $1 \text{ kT}$ . We can improve the estimate of the free-energy change by taking the mean of the Jarzynski values for folding and unfolding to obtain a value of  $\Delta G = 110.3 \text{ kT}$ . Because the process is not far from reversible, the mean of the directly measured work values for unfolding and refolding ( $110.2 \text{ kT}$ ) is also a good measure of  $\Delta G$ . Of course, Jarzynski's method can still provide  $\Delta G$  even when both unfolding and refolding cannot be measured. To obtain the free-energy change for unfolding the RNA hairpin at zero force we subtract as shown before, the stretching of the handles and RNA single strand to get  $\Delta G^\circ = 62.8 \pm 1.5 \text{ kT} = 37.2 \pm 1 \text{ kcal/mol}$ .

Using force to unfold a molecule means that, in principle, we can pull slowly enough so that the process takes place quasi-statically and therefore reversibly. However, two considerations that make this approach impractical are drift in the apparatus, which can degrade the quality of the data, and the total time required to obtain reproducible values of reversible work. In practice, if the average dissipated work is only a few  $\text{kT}$ , sometimes it is quicker and more efficient to do many pulls rapidly and to use Jarzynski's equation to obtain  $\Delta G$ , than to do a single very slow pull.

For processes far from equilibrium that can be measured in both the forward and reverse direction, a method based on Crooks fluctuation theorem (Crooks, 1999) provides a more robust way of obtaining free energies.

### 3.2.4.2 Crooks fluctuation theorem (Crooks, 1999)

Crooks fluctuation theorem states that there is a relation between the thermal fluctuations in a forward trajectory and a reverse trajectory for the same process. The probability of a trajectory with work value ( $w$ ) done in the forward direction is related to the probability of work value obtained ( $-w$ ) in the reverse direction by:

$$\frac{P_{\text{forward}}(w)}{P_{\text{reverse}}(-w)} = e^{(w - \Delta G)/kT}. \quad (3.16)$$

The value of the work for which the magnitudes of the two probability distributions are equal (the value for which the distributions intersect), is the value of the work equal to the free energy of the system. It is intuitively reasonable that the trajectory with the same value of work for the forward and reverse process corresponds to the reversible trajectory. However, there is much more substance to the Crooks fluctuation theorem. It states that the entire forward distribution can be calculated from the measured reverse distribution. Of course for work values far from the reversible value ( $\Delta G$ ), the forward or reverse trajectories will be so rare that they will be difficult to measure. Integration of Eq. (3.16) over all values of work gives

$$I = \langle e^{(w - \Delta G)/kT} \rangle, \quad (3.17)$$

i.e. Jarzynski's identity.

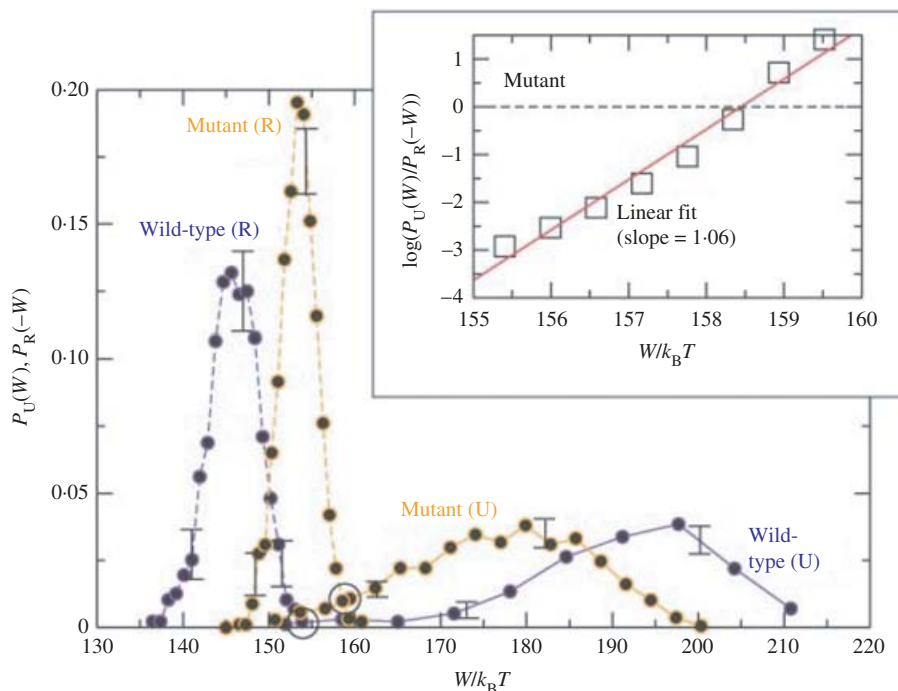


**Fig. 5.** Free-energy recovery by Crooks fluctuation theorem (adapted from Collin *et al.* 2005). Unfolding (solid lines) and refolding (dashed lines) work distributions for wild-type (purple) and mutant (orange) S15 three-helix junctions are shown. The intersections of the distributions for folding and unfolding (large empty circles) provide  $\Delta G$  for the reactions. Over 900 and 1200 trajectories were collected for the wild-type and mutant RNA, respectively. The inset shows the logarithmic ratio of unfolding to refolding work probabilities as a function of total work done on the molecule. The solid line is a fit to Eq. (3.16).

Figure 5 shows measured work distributions for the unfolding and refolding of a three-helix junction from a small subunit ribosomal RNA (900 repetitions), and its 1-bp mutant (1200 repetitions) (Collin *et al.* 2005). The unfolding and refolding processes are far from equilibrium; the average dissipated work for unfolding is over 30 kT, and for refolding it is over 15 kT. Jarzynski's equation is impractical, but the Crooks fluctuation theorem is applicable. The crossover of the distributions and thus the free energies can be determined to  $\pm 0.3$  kT. Equation (3.16) shows that the logarithm of the ratio of probabilities is linear in  $w$  with intercept equal to  $\Delta G$ . The inset in Fig. 5 illustrates this behavior for the mutant. The difference in free energies between mutant and wild-type molecules is  $\Delta\Delta G = 3.8 \pm 0.6$  kT. Subtracting the free energies of stretching the handles and single strand RNA (identical for both molecules) gives  $\Delta G^{\circ}$  at zero force =  $57 \pm 1.5$  kT for the wild type. Thus, using the Crooks fluctuation theorem on a molecule whose kinetics is slow and its unfolding is far from reversible, we can obtain precise Gibbs free-energy changes. Changes in free energy,  $\Delta\Delta G$ , of 7% (a change of 1 bp in 34 bp) could be detected.

The increase in uncertainty for the free-energy value at zero force compared to the value at the measured force is caused by the uncertainty in the stretching correction. However, values of changes in free energies,  $\Delta\Delta G$ , between mutants with the same number of nucleotides do not depend on any stretching calculations. Thus, force unfolding can be particularly useful for

determining changes caused by mutations, by binding ligands such as magnesium ions (Collin *et al.* 2005), or by changing solvent.

## 4. Kinetics

### 4.1 Measuring rate constants

#### 4.1.1 Hopping

When force is held constant at a critical force, a RNA can display bi-stability, since the energy levels of folded and unfolded states are equal. The molecule has nearly equal probabilities to exist in unfolded and folded states, and hops back and forth between the two. Therefore, reaction kinetics and mechanism can be studied by monitoring the lifetimes of the molecule in each state. Because only one molecule is observed, reaction trajectories can be followed directly; there is never more than one species contributing to the signal at one time and thus the ensemble average of bulk experiments can be avoided. Figure 6a shows extension *versus* time traces of a simple RNA hairpin undergoing a transition between a folded and an unfolded state. The average force on the molecule is held constant by force feedback, while the molecule hops back and forth between the two species, as indicated by the extension. We see a distribution of lifetimes as expected for a stochastic kinetic process. The average lifetimes of each species for this first-order process are simply equal to the inverse of the rate coefficients for exiting that species to form the other. The probability of a lifetime between  $\tau$  and  $\tau + d\tau$  is distributed exponentially;  $P(\tau)$ , is the probability density.

$$P(\tau)d\tau = \kappa e^{-\kappa\tau} d\tau, \quad (4.1)$$

We can thus simply calculate the mean of the lifetimes, which is equal to the reciprocal of the rate constant.

$$\langle \tau \rangle = \int_0^{\infty} \tau P(\tau) d\tau = 1/\kappa. \quad (4.2)$$

The probability that the reaction has occurred before time  $t$  is the integral of  $P(\tau)$  from 0 to  $t$ , thus the probability that the reaction has *not* occurred,  $P(t)$ , is  $e^{-\kappa t}$ . Therefore, we can obtain the rate constant,  $\kappa$ , from the slope of a plot of the logarithm of the fraction of lifetimes greater than time  $t$  *versus*  $t$ .

$$\ln P(t) = -\kappa t, \quad (4.3)$$

The rate constants from the slope and from the mean of the lifetimes should agree. If the  $\ln$  plot is not linear, or agreement among the  $\kappa$ 's is not found within experimental error, it suggests that intermediates are present that are not seen. Figure 6b shows log plots of the fraction of molecules unreacted during folding and unfolding. We see linear plots with rate constants from the slopes of  $43 \pm 1 \text{ ms}^{-1}$  for unfolding and  $33 \pm 1 \text{ ms}^{-1}$  for folding. The rate constants from the mean of measured lifetimes agree within 10%.

To illustrate the difference between ensemble kinetics and single-molecule kinetics, let us consider the mechanism shown in Fig. 7. Four species are involved in a branched path; six rate constants determine the kinetics. The calculated concentration of each species is plotted *versus* time for a chosen set of rate constants. Clearly, it will be difficult to measure the concentrations,

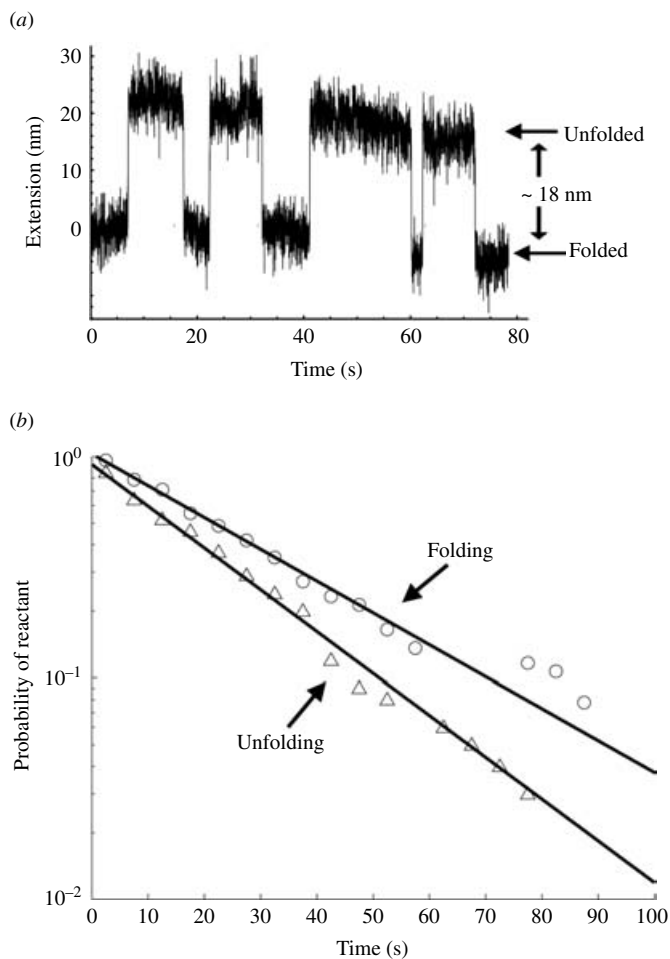


**Fig. 6.** Hopping kinetics of a hairpin (Li *et al.* 2006). (a) A time trace of the extension of a TAR RNA hairpin that hops between folded and unfolded states at a constant force of 12.4 pN in 250 mM KCl (pH 22 °C). A change in extension of about 18 nm occurs as the 22-bp helix forms and is broken. (b) The probability that the reaction has not occurred (fraction of reactant present) is plotted as a function of time. Lifetimes of the unfolded or folded states ( $> 100$  observations each) are binned in 5 s intervals to generate the probability density function and the cumulative probability. The mean lifetime of the unfolded state gives the folding rate; the mean lifetime of the folded state gives the unfolding rate. The solid lines represent fits to a single exponential. The first-order rate constant for folding the RNA is  $43 \pm 1 \text{ ms}^{-1}$ , and that for unfolding is  $33 \pm 1 \text{ ms}^{-1}$ . Rare lifetimes over 100 s were observed for the folding reaction; these points do not fit the single exponential and are not shown.

because all species are present at the same time. Even if the concentrations are measurable, extracting a unique set of rate constants from the data will be very difficult. In contrast, with a single molecule experiment (Fig. 8), the signal (extension) is from a single species at one time. A simulated hopping experiment is shown in Fig. 8 illustrating a short region of a possible time-dependent signal. The average lifetime of each species is the reciprocal of the sum of rate constants for all channels leaving that species. If there is a single channel leaving a species, the rate constant is directly measured from the average lifetime. If more than one channel exists ( $B \rightarrow A$  or  $B \rightarrow C$  or  $B \rightarrow D$ ), the relative probabilities of each channel must be measured to

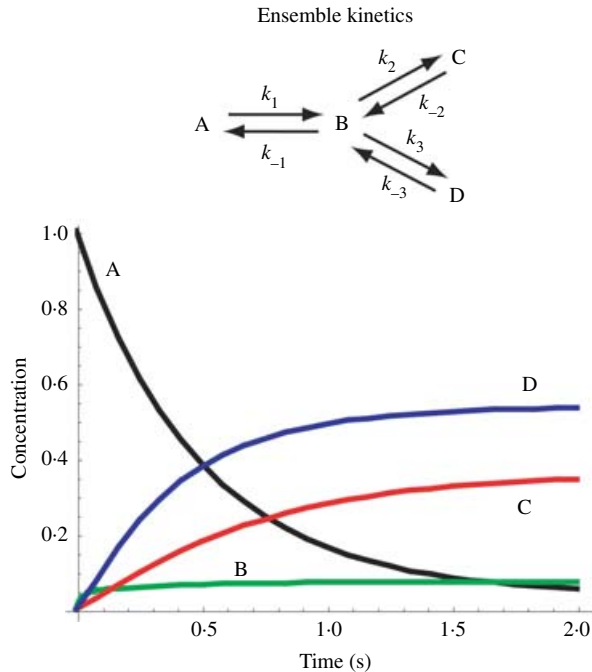


**Fig. 7.** The concentrations *versus* time of four species that follow the kinetic scheme shown. Note that in the usual ensemble experiments all four species are present at all times; and there is no unique way to extract the rate constants from the measured data.

obtain the individual rate constants. For example in Fig. 8, the ratio of probability of channel  $B \rightarrow C$  and channel  $B \rightarrow D$  is  $k_2/k_3$ . In principle all six rate constants can be determined from a hopping experiment that identifies each transition  $\sim 100$  times. Of course in practice, the species may have similar extension, the lifetimes may be too short or too long for the instrumentation, and noise will hide or emulate transitions. An advantage of the stochastic nature of kinetics is that although the average lifetime may be too short to detect, longer lifetimes will occur. For example, 5% of lifetimes will be more than three times as long as the mean lifetime, and 1% will be more than 4.6 times as long. Furthermore, each reaction step will have different force-dependent kinetics that can allow the identification and quantitation of the kinetic mechanism.

Note that  $P(t)$ , the probability that the reaction has not occurred, is calculated by summarizing many single molecule events; hence,  $P(t)$  is equivalent to the concentration of the reactant measured in a bulk experiments. If the mechanism of the reaction is the same for the single-molecule reaction and the bulk reaction, the rate constants measured by both methods should be equal. However, in general a reaction induced by force will have a different mechanism than one induced by increase of temperature or concentration of denaturant. Other contributions to differences between bulk and single-molecule experiments are inactive, impurity and damaged species that may exist in the bulk measurements, but are not detected in the single-molecule experiments.

#### 4.1.2 Force-jump, force-drop

Unfolding/folding a complex molecule may involve several steps, each of which can occur at different forces. It is likely that at any particular force, rate constants of these steps vary by several

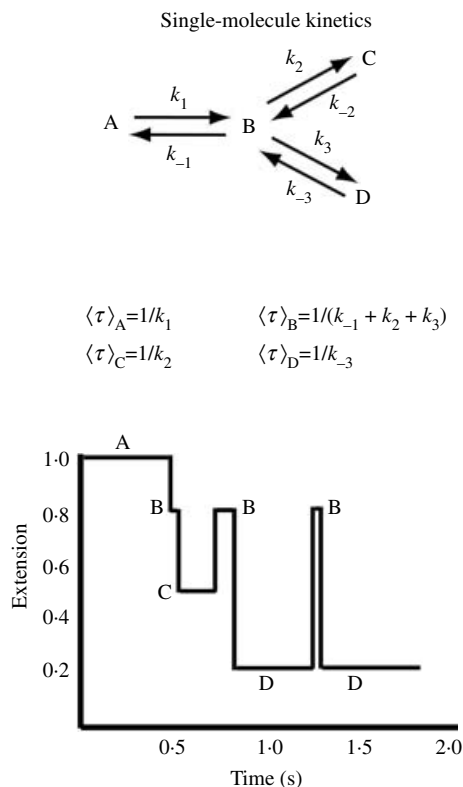


**Fig. 8.** The same scheme used in Fig. 7 studied one molecule at a time. Obviously, only one species is present at any time. Each rate constant is uniquely characterized by the average lifetime of each species, as it transits to another species.

orders of magnitude, thereby making the hopping experiment impractical. One can then employ a force-jump or force-drop protocol, in which tension on the molecule is rapidly changed between values. At each set force, a particular reaction step is studied; the occurrence of the transition is indicated by the extension change, just as in the hopping experiments. Such a protocol allows us to study the sequential unfolding/folding reaction of a tertiary RNA structure, identify the rate-limiting steps and measure the rate constants of each step (P. Li *et al.* unpublished observations). In Fig. 9, we present an example of applying the method to study the unfolding/refolding kinetics of a RNA hairpin (Li *et al.* 2006). The force is first quickly raised to a value where the lifetimes of the folded species are measurable. After the unfolding transition occurs and the lifetime of the folded species at this force is measured, the force is increased further to insure complete unfolding. Then the force is quickly dropped to a value where lifetimes of the unfolded RNA are measurable. The procedure is repeated enough times ( $\sim 100$ ) to obtain sufficient statistics. From the measured lifetimes, rate constants can be calculated as described in the hopping experiments [Eq. (4.3)].

#### 4.1.3 Force-ramp

Rate constants can be obtained from the distribution of forces where a transition (rip) occurs as force is increased with time in a force-ramp experiment (Evans & Ritchie, 1997). Increasing force

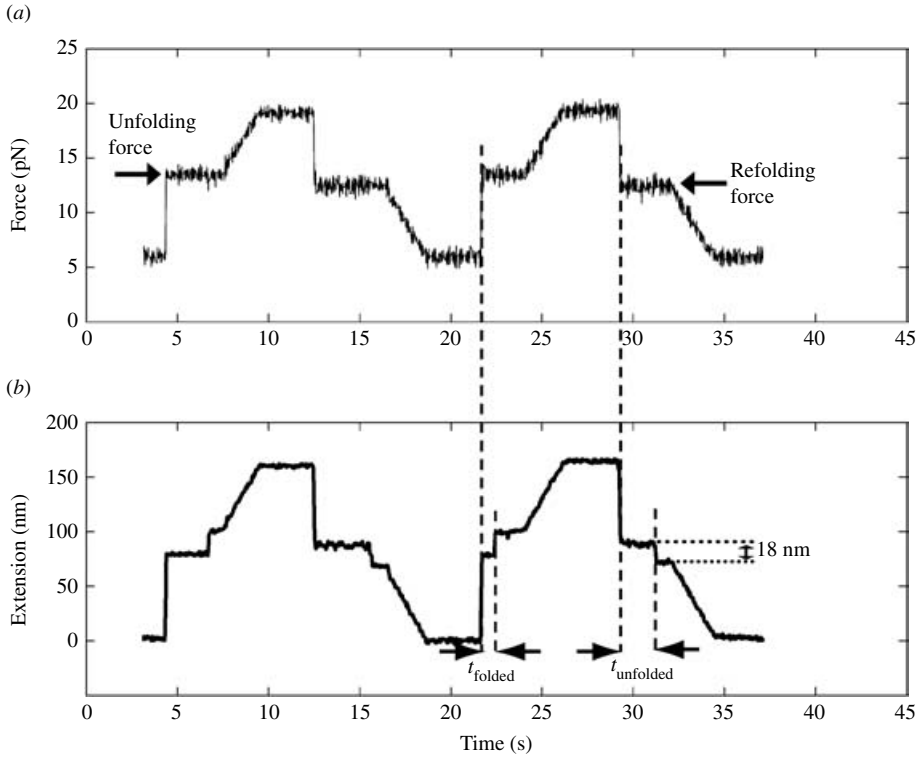


**Fig. 9.** Examples of force-jump-drop experiments (adapted from Li *et al.* 2006). (a) A time trace of force in two force-jump-drop events. Each cycle starts at 6 pN, at which the hairpin is folded. The force is quickly raised to 14 pN and held constant until the unfolding occurs. After the unfolding, the force is further ramped to 20 pN and held there for 3 s to insure complete unfolding. Then the force is quickly dropped to 12.7 pN to monitor the refolding. In the last step, the force is decreased to 6 pN. (b) A time trace of extension for the same experiments shown in panel (a). At the unfolding force, the extension of the molecule remained constant until the unfolding, at which time the extension suddenly increased by  $\sim 18$  nm. At the refolding force, the formation of the hairpin was indicated by the quick decrease in the extension. Lifetimes of the species,  $t_{\text{folded}}$  and  $t_{\text{unfolded}}$ , were used to calculate the rate constants of unfolding and refolding, respectively.

favors the species with the longer extension, thus speeding unfolding reactions and slowing folding reactions. From transition-state theory a rate constant depends exponentially on the free-energy difference between the reactant and the transition state (assumed to be in rapid equilibrium with reactant). As Gibbs free energy is equal to the reversible mechanical work, we write

$$k(F) = k_0 e^{F\Delta X^\ddagger / kT}, \quad (4.4)$$

The force is  $F$ , the distance to the transition state is  $\Delta X^\ddagger$ , and  $kT$  is Boltzmann's constant times temperature.  $k_0$  is the rate constant of the mechanical unfolding process at zero force. In general, however, the unfolding pathway will be different for thermal or solvent induced reactions and for mechanically-induced processes, so  $k_0$ , as expressed in Eq. (4.4), is not directly comparable with the usual bulk measurements. The time dependence of the probability that the reaction has not occurred is

$$\frac{dP(t)}{dt} = -k(F)P(t), \quad (4.5)$$

In a force-ramp experiment the force increases approximately linearly with time ( $F = rt$ ) with  $r$  the loading rate in pN/s. Therefore,

$$\frac{dP(t)}{P(t)} = -k_0 e^{(\Delta X^\ddagger / kT)rt} dt, \quad (4.6)$$

Integration of Eq. (4.6) from time zero to  $t$  gives

$$\ln P(t) = \frac{k_0}{rb} (1 - e^{brt}) \cong -\frac{k_0}{rb} e^{brt}, \quad (4.7)$$

with  $b = \Delta X^\ddagger / kT$ . The relevant range of Eq. (4.7) is when the probability of the reaction is significant; this means that the exponential term is large compared to 1. We thus obtain for the force dependence of the reaction

$$\ln P(F) = -\frac{k_0}{rb} e^{bF}, \quad (4.8)$$

Equation (4.8) is a useful approximation when  $e^{bF} > 10$ ; this means  $F > 2$  pN for  $\Delta X^\ddagger = 5$  nm. To obtain  $k_0$  and  $b = \Delta X^\ddagger / kT$  for loading rate  $r$  we write Eq. (4.8) in a linear form.

$$\ln[r \ln(1/P(F))] = \ln \frac{k_0}{b} + bF, \quad (4.9)$$

Many force-ramp experiments are done with chosen loading rate, and the distribution of rips as a function of force is determined. The fraction of rips that occur after force  $F$  is  $P(F)$ . The slope of a plot of Eq. (4.9) gives the distance to the transition state; the intercept plus slope give  $k_0$ .

Rate constants for unfolding/refolding a TAR RNA hairpin have been measured using the three different methods: hopping, force-jump/drop, and force-ramp (Li *et al.* 2006). Satisfactory agreement among these different experiments was found.

#### 4.1.4 Instrument effects

We have discussed measurements of kinetics as abrupt increases or decreases in RNA extension, corresponding to the movement or re-positioning of the bead in the laser trap. Clearly the fastest change that we can measure is limited by how fast the bead can move. The motion of the bead is determined by its corner frequency, whose inverse gives the relaxation time of the bead in the trap. The corner frequency is given by the ratio of the effective stiffness of the potential acting on the bead to the friction or drag coefficient of the bead. It thus depends on the size of the bead, the viscosity of the medium, stiffness of the optical trap, and the flexibility of the molecular handles. A bead of radius  $1 \mu\text{m}$  in an aqueous solution in a laser trap with stiffness  $0.1 \text{ pN} \cdot \text{nm}$ , has a corner frequency of  $\sim 5 \text{ kHz}$ . We recall that at the corner frequency the response of the bead is one half what it is at low frequencies. The rate constants that we typically measure are in the range between  $0.1$  and  $10 \text{ s}^{-1}$ , so we do not expect much interference from the motion of the bead in the trap. The effects of the beads on the apparent kinetics of unfolding/refolding can be simulated (Manosas & Ritort, 2005; M. Manosas *et al.* unpublished observations). Since the length of the handles determines their compliance and, therefore, the effective stiffness of the trap, we have measured the unfolding/refolding kinetics for a RNA hairpin using three different handle lengths (1 kb, 3 kb, 10 kb) (J.-D. Wen *et al.* unpublished observations). The rate constants

agreed within a factor of four; the longer, more flexible handles gave values closer to the calculated rates for the unconstrained RNA. However the ‘softer’ handles also produced a noisier signal. Thus, there is no absolute optimum length, or optimum stiffness, for handles. Their choice depends on the magnitudes of the kinetic rates that are being measured, and the sizes of the transitions involved.

The apparent kinetics also depends on the degree of control of the force during the experiment (J.-D. Wen *et al.* unpublished observations). We measure hopping and force-drop or force-jump at constant average force, but the speed of the instrumental force feedback control can affect the kinetic results. Passive mode kinetic measurements, where both extension and force are allowed to change and fluctuate during the reaction, can also be obtained. In principle, instrumental effects, as those described in this section, can be simulated to obtain the true molecular rates.

As should be expected, handle length, trap stiffness, force feedback, etc., do not affect the thermodynamic significantly (J.-D. Wen *et al.* unpublished observations). Experimentally and theoretically the reversible mechanical work and free energies should be and, in practice are, independent of instrumental parameters.

## 4.2 Kinetic mechanisms

### 4.2.1 Free-energy landscapes

The thermodynamics and kinetics of RNA secondary structures can be described satisfactorily by a nearest-neighbor model (Tinoco *et al.* 1971). The free energy of a folded structure is written as the sum of free energies of double-stranded helices plus free energies of hairpin loops, internal loops and bulges. The difference between an internal loop and a bulge is that in a bulge there are no bases unpaired on one of the strands. The free energies of loops and bulges are usually assumed to be independent of sequence, except for special sequences. The free energy of a helix depends on its sequence only through nearest-neighbors interactions. There are ten Watson–Crick nearest-neighbors, but base-base mismatches increase the number of different nearest-neighbor free energies significantly. Tables of nearest-neighbor free-energy values at 37 °C are available (Mathews *et al.* 1999, 2004), as are values of  $\Delta H^\circ$  and  $\Delta S^\circ$  (although these are less reliable).

The nearest-neighbor model provides equilibrium constants for forming each base pair. It thus gives the ratio of kinetic rate constants for forming and breaking each base pair. Although at present we do not have the temporal or spatial resolution to detect single base-pair opening and closing (times of  $<0.1 \mu\text{s}$ ; distances of 0.1 nm), we can write any mechanism and solve for the rate-determining – measurable steps.

In force unfolding of a hairpin – a stem-loop – the molecule is assumed to break 1 bp at a time starting from the 5′- and 3′-ends where the force is applied (Cocco *et al.* 2003a). Refolding can be more complicated. The first base pair formed need not be the one that closes the loop, and it need not even be a base pair that is in the native folded structure. Figure 10 shows the calculated increase in free energy for a hairpin (P5ab) using the nearest-neighbor model as the RNA is unfolded 1 bp at a time. The free energy,  $G_i[F]$ , in the force representation of each partially unfolded species  $i$  (relative to the completely folded hairpin,  $G_{\text{HP}}[F]$ ) as a function of force is

$$\Delta G_i[F](F) = G_i[F](F) - G_{\text{HP}}[F](F),$$

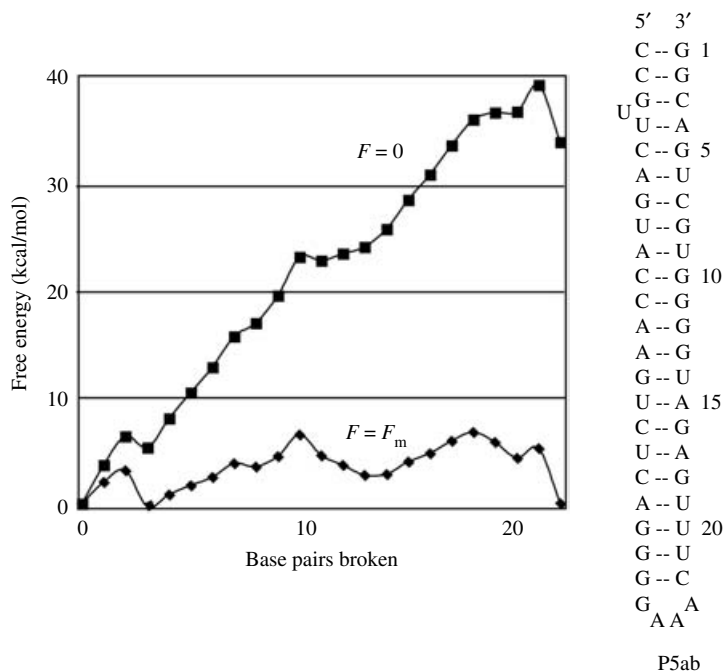


**Fig. 10.** Calculated free-energy landscape at 25 °C for RNA hairpin P5ab at zero force and at  $F_m$ , the melting force. At zero force the free energies are calculated from nearest-neighbor values (Mathews *et al.* 1999); at the  $F_m$  the WLC model is used to obtain the effect of force on each partially unfolded species. At zero force the hairpin is the only species present. At  $F_m$  the species present in significant amounts are now the hairpin, the single strand, and the hairpin with 3 bp broken caused by the destabilizing effect of the bulged U. (This figure from Tinoco, 2004.)

The free energy of the hairpin decreases linearly with force  $-(FX_{HP})$ , as we assume that it is rigid;  $X_{HP}$  is taken as 2 nm (the diameter of a double helix). Then

$$\Delta G_i[F](F) = \Delta G_i^\circ(F=0) + \int_0^{X_{SS}} F' dX_{SS} - FX_{SS}, \quad (4.10)$$

$\Delta G_i^\circ(F=0)$  is the positive free energy of breaking  $i$  base pairs from the end of the intact hairpin; it is shown in Fig. 10. The second term is the positive stretching free energy for the single-stranded ends of the partially unfolded RNA; we use the WLC for  $F$ . The last term is negative; it stabilizes the unfolded species in direct proportion to the extension of the single-strand ends,  $X_{SS}$ . The magnitude of  $X_{SS}$  increases with each base pair broken; its value is obtained from the contour length ( $L=0.59 \cdot 2i$  nm) of the single-strand ends formed, and the WLC model. As Eq. (3.27) is the difference in free energy between each partially unfolded species and the folded hairpin, the terms in  $FX_{HP}$  cancel. However, when the last base pair is broken and only the single strand exists, the last term in Eq. (3.27) is replaced by  $-(FX_{SS} - FX_{HP})$ .

At zero force the free energy increases steadily as each base pair is broken. There are decreases as the U bulge is reached after base pair 3; as the two A•G's occur after base pair 11, and as the hairpin loop is released. With increasing force, each partially unfolded species is preferentially stabilized because its extension is longer than the folded hairpin. At a critical force the force representation of free energy,  $\Delta G[F]$ , is the same for the folded hairpin and the unfolded single

strand. This means that the two species are in reversible equilibrium at this force; their equilibrium constant = 1. The critical force is designated as  $F_{1/2}$  or  $F_m$ , the melting force. Equation (10) shows the free-energy landscape at  $F_m = 17.0$  pN where the single strand and hairpin are calculated to have equal free energies; the experimental value is  $14.5 \pm 1$  pN. Given the approximations in the nearest-neighbor model and parameters, and in the WLC model applied to a few nucleotides, the agreement between measured and calculated melting forces is encouraging.

#### 4.2.2 Kinetics of unfolding

We can use the nearest-neighbor model to understand the kinetics of unfolding and refolding of a hairpin. A (positive) free-energy value,  $\Delta G^\circ(NN)$ , which depends on the neighboring base pair, exists for each base pair broken from the end of a helix. Breaking a base pair that releases a loop decreases the free energy,  $\Delta G^\circ(\text{loop})$ , which is assumed to depend only on the number of nucleotides released. The ratio of rate constants for opening and closing a base pair at zero force – equal to the equilibrium constant for breaking a base pair – is

$$\frac{k(\text{open})}{k(\text{close})} = e^{-\Delta G/kT}, \quad (4.11)$$

The force dependence of each rate constant depends on the distance to the transition state as given by a Bell-like equation (Bell, 1978)

$$k(F) = k_0 e^{F\Delta X^\ddagger/kT}, \quad (4.12)$$

For these elementary steps,  $k_0$  is the rate constant at zero force; it is not dependent on mechanism. We use the assumption originally made by Cocco *et al.* (2003a) that  $\Delta X^\ddagger$  for opening a base pair is zero, therefore the opening rate constants are independent of force. The rationale for this assumption is that hydrogen bonds are very short range ( $\sim \text{\AA}$ ). The closing rate constants do depend on force, with the distance to the transition state equal to the change in extension.

$$\Delta X^\ddagger(\text{close}) = \Delta X(\text{close}) - \Delta X^\ddagger(\text{open}) = \Delta X(\text{close}), \quad (4.13)$$

The value of  $\Delta X(\text{close})$  is negative.

Figure 11 shows a mechanism and the form of the rate constants for the elementary steps. Breaking a base pair in a helix is independent of force, but dependent on nearest-neighbor sequence. Closing a base pair in a helix depends on force through a distance to the transition state of about 1 nm [a decrease in contour length of  $2(0.59)$  nm]. Breaking a base pair that opens a loop is independent of force and sequence; it depends on the number of nucleotides released. Closing the base pair that forms a loop depends on the force and the size of the loop. Because  $\Delta X$  is negative, the larger the loop the slower the loop closing rate constant. Note that the kinetics in this model depends on only two adjustable parameters:  $k_{z0}$ , the rate constant for forming (zipping) a base pair in a helix at zero force, and  $k_{l0}$ , the rate constant for forming the base pair that closes a loop at zero force.

The kinetics of the single-molecule unfolding/refolding reaction are characterized by a set of coupled linear differential equations that can be solved by standard methods to obtain the time dependence of each species as a function of force (Steinfeld *et al.* 1989). For  $N$  species  $N$  relaxation times are obtained that are functions of all the individual rate constants. In all the calculations that we and others have done (Cocco *et al.* 2003a; Viereggs & Tinoco, 2006), one relaxation time (the rate determining one) is slower by at least two orders of magnitude relative to

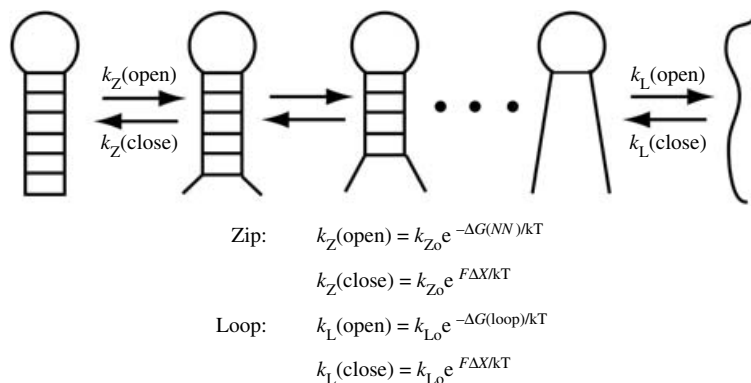


**Fig. 11.** A simple kinetic mechanism for the unfolding of RNA secondary structure. There are four elementary steps, but only two are independent because the ratio of rate constants equal equilibrium constants. The assumptions are that helix free energies depend only on the nearest-neighbor base pairs, and loop free energies depend only on loop size. Base-pair opening is assumed to be essentially independent of force because the distance to the transition state for base-pair opening is of order 0.1 nm (Cocco *et al.* 2003a).

the others. Thus the appearance or disappearance of a species has a single exponential time dependence.

The effects of instrumental parameters, such as laser trap stiffness, bead size, handle length, etc., on the molecular rate constants can be modeled (M. Manosas *et al.* unpublished observations). The simulations allow one to extract the molecular rate constants from the apparent, measured kinetics (J.-D. Wen *et al.* unpublished observations).

Figure 12a shows single exponential curves for the unfolding of TAR RNA at two different forces. The curves are the fraction of lifetimes less than time  $t$  plotted *versus*  $t$ . The rate constants are obtained from the least squares best fit to a single exponential, or alternatively, from the mean of all lifetimes. Figure 12b shows linear plots of the logarithm of the rate constants *versus* force. The slope depends on the distance to the transition state. The intercept at zero force should not be interpreted as the logarithm of the rate constant at zero force; it should not be directly compared with thermal or denaturant unfolding kinetics. The distance to the transition state must decrease as the force decreases so a linear extrapolation is not correct; also the mechanism of the reaction may be very different for force unfolding.

Woodside *et al.* recently measured the thermodynamics and kinetics of 20 different DNA hairpins with different stem lengths, G•C content and loop sizes (Woodside *et al.* 2006). Their work illustrates how folding free energies and rate constants critically depend on the sequences and structures of the hairpins. As more experimental data are obtained and more calculations are done (Cocco *et al.* 2003a; Vieregg & Tinoco, 2006), we expect that folding kinetics of DNA and RNA hairpins under tension can be accurately predicted.

## 5. Relating force-measured data to other measurements

### 5.1 Thermodynamics

Measurements of the change in thermodynamic properties caused by a reaction can only be compared if the initial and final states are the same for the measurements. Figure 13 illustrates

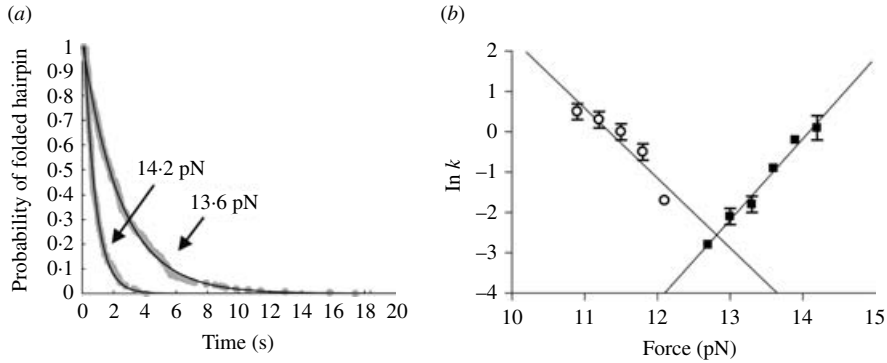
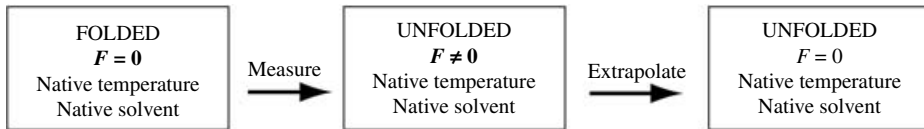
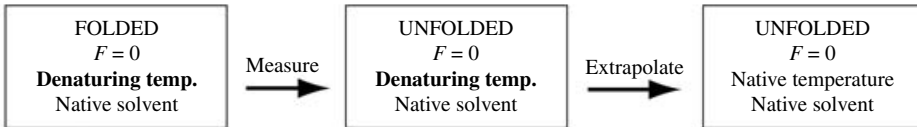


**Fig. 12.** Force-jump kinetic data for the unfolding of TAR RNA (adapted from Li *et al.* 2006). (a) Plots of fraction of folded RNA *versus* time at 13.6 pN and 14.2 pN; the curves fit well with single exponentials consistent with first-order kinetics. (b) Plot of the logarithm of the rate constants *versus* force for unfolding and refolding. The slopes of the linear plots give the distances to the transition state from the folded state ( $\Delta X^\ddagger = 8.2$  nm), and from the unfolded state ( $\Delta X^\ddagger = 8$  nm). The transition state is roughly halfway between the folded and unfolded species.

Force unfolding:



Thermal unfolding:



Solvent unfolding:

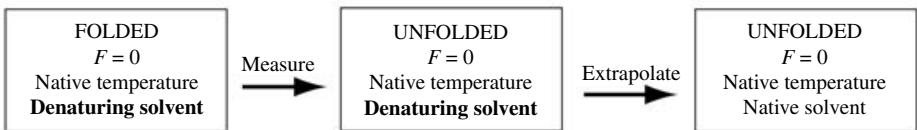


**Fig. 13.** Schematic diagram illustrating the differences in initial and final states for force, thermal, and solvent unfolding. For each experiment the environment is adjusted to produce measurable amounts of two species, such as folded and unfolded. Then the ratio of species is measured to give an equilibrium constant and free energy, or the work necessary to convert one species to the other is measured.

the different states for the usual ways of measuring the free energy of unfolding RNA (or protein).

- (1) In force unfolding the RNA starts in a native solvent and temperature, then the force is increased until the molecule unfolds. If the same force is obtained on refolding the RNA (the reaction is reversible), the product of force times the change in distance is equal to the

reversible work, and thus the Gibbs free-energy change at the reversible force. The final state is the stretched single strand. We obtain the Gibbs free-energy change for the reaction from folded to stretched, unfolded state at the reversible force, and chosen temperature and solvent. The free energy can also be obtained from the equilibrium constant for folded and unfolded states at a constant force in hopping experiments. The molecule transits between states, and the ratio of average lifetimes in each state is the equilibrium constant. The Gibbs free energy at that force is calculated from the measured equilibrium constant. To calculate the free energy at any other force, the WLC equation [Eq. (3.9)] is used to calculate the entropy (free energy) change of the single strand as the force changes.

- (2) In thermal unfolding the RNA starts in a native solvent and zero force, then the temperature is increased until a measurable fraction of unfolded species is obtained, and an equilibrium constant can be determined. The Gibbs free energy at that temperature is calculated from the measured equilibrium constant. Usually the equilibrium constant is measured as a function of temperature to obtain a linear temperature dependence for the standard free energy,  $\Delta G^\circ = \Delta H^\circ - T\Delta S^\circ$ . The free energy is extrapolated to any temperature assuming the enthalpy and entropy are independent of temperature.
- (3) In solvent unfolding the RNA starts in a native temperature and zero force, then the denaturant is increased until a measurable fraction of unfolded species is obtained, and an equilibrium constant can be determined. The Gibbs free energy at that temperature is calculated from the measured equilibrium constant. The equilibrium constant is measured as a function of concentration of denaturant so as to be able to extrapolate the free energy to zero denaturant concentration.

Clearly, all three methods involve different assumptions, and all three methods require extrapolation to reach the same initial and final states. Nevertheless, the equilibrium free energy obtained should be independent of the method used. A direct comparison of the force-method with either bulk method would be to choose a temperature and solvent where both folded and unfolded species exist at zero force. Then force could be increased to be able to measure hopping. Equilibrium constants measured by hopping and extrapolated to zero force could be compared with the usual bulk methods (absorbance, fluorescence, circular dichroism, etc.). All measurements would thus be at the same temperature and solvent.

Direct comparison of free energies from force unfolding experiments with bulk methods has not been done. Extrapolation of unfolding free energies measured at 15–20 pN to zero force requires knowledge of the free energy of stretching the RNA single strand. The stretching free energies can be 20–30% of the measured values, and have been calculated using the WLC model. The zero-force free energies have been obtained from Mfold (Zuker, 2003), which is based on thermal melting data (Mathews *et al.* 1999, 2004) and the nearest neighborhood approximation (Tinoco *et al.* 1971). In the case of TAR RNA, we found that our value of  $\Delta G^\circ$  (Li *et al.* 2006) was  $\sim 20\%$  lower than the Mfold value. The approximations used in the two methods make it difficult to decide which value is more correct. Differences in free energies caused by mutations, ligands, or salt concentrations will always be more accurate than absolute values.

The previous discussion has implicitly assumed a two-step reaction: folded-to-unfolded. More complicated reactions with many intermediates can be studied. As long as initial and final states can be specified, and equilibrium can be established between them, thermodynamic values can be obtained. In bulk methods equilibrium can usually be established although the kinetics may

require hours before equilibrium is reached. In single-molecule methods it is impractical to wait hours for equilibrium to be established; however, we have described how equilibrium free energies can be obtained from non-equilibrium reactions (Jarzynski, 1997; Crooks, 1999; Liphardt *et al.* 2002; Collin *et al.* 2005).

## 5.2 Kinetics

In kinetics experiments the mechanism of the reaction determines the kinetics. The mechanisms, in general, will be different for force unfolding, thermal unfolding, and denaturant unfolding. Therefore, we will expect different apparent kinetics for the bulk methods and the single-molecule force method. Recently, detailed folding kinetic schemes for a small hairpin under various temperatures and forces have been discussed (Hyeon & Thirumalai, 2005, 2006).

We generally observe two-state, first-order kinetics with lifetimes that display a single exponential time distribution. The lifetimes fit a single kinetic rate constant that can be compared directly with bulk-measured kinetics. The measured rate constant is a function of the rate constants of the individual elementary steps in the reaction. The elementary steps include the making and breaking of individual base pairs, the binding and releasing of ions, and so forth. The mechanism for force unfolding is expected to be the simplest, because the force is local and disrupts one part of the molecule before the rest of the molecule feels the force. In L-21 (Onoa *et al.* 2003) the P4–P6 domain unfolds last at the same force as the isolated P4–P6 because the catalytic core has to unfold before the force applied to the 3'- and 5'-ends is propagated to the P4–P6 domain. In thermal or solvent unfolding all domains experience the global effects. Similarly, a hairpin will unfold from the end of the helix when force is applied, but will melt from the loop end as well, when the temperature or denaturant is increased. Calculation of the rate constants for unfolding a simple hairpin thermally and by force illustrate the differences (Tinoco, 2004). Although the elementary kinetic steps of breaking and forming base pairs are similar, the rate-determining (measured) kinetics are faster for thermal unfolding because there are more paths leading to the single strand.

It is clear that thermodynamic results ( $\Delta G$ ,  $\Delta H$ ,  $\Delta S$ ) obtained by force perturbations, or thermal or solvent perturbations are equally pertinent to biological processes. The kinetic results are less clear. The distance to the transition state can only be measured by force. If this distance is short ( $\sim 1$  nm), does that mean the transition state in a thermal reaction will be close to the starting species? The answer is presumably yes, if the mechanisms for the two reactions are similar. For example, in kissing hairpin loops there is a short distance to the transition state when the loops break (P. Li *et al.* unpublished observations). We expect the transition state for the thermally unfolded kissing loops also to be close to the folded state. Pulling on the ends of a RNA may mimic the effect of a ribosome pulling on the 5'-end of a mRNA during translation. Similarly, the mechanical force exerted by a helicase on unfolding a RNA hairpin (Dumont *et al.* 2006) has characteristics in common with the force applied by laser tweezers.

Force, and single-molecule methods in general, are new tools to apply to biological problems. We expect rapid advances in the next few years.

## 6. Acknowledgements

The authors are supported by NIH grants GM-10840 (I.T.) and GM-32543 (C.B.).

## 7. References

- ABBONDANZIERI, E., GREENLEAF, W., SHAEVITZ, J., LANDICK, R. & BLOCK, S. (2005). Direct observation of base-pair stepping by RNA polymerase. *Nature* **438**, 460–465.
- ABELS, J., MORENO-HERRERO, F., VAN DER HEIJDEN, T., DEKKER, C. & DEKKER, N. (2005). Single-molecule measurements of the persistence length of double-stranded RNA. *Biophysical Journal* **88**, 2737–2744.
- ALLISON, D., HINTERDORFER, P. & HAN, W. (2002). Biomolecular force measurements and the atomic force microscope. *Current Opinion in Biotechnology* **13**, 47–51.
- ASHKIN, A. (1998). Forces of a single-beam gradient laser trap on a dielectric sphere in the ray optics regime. In *Methods in Cell Biology*, vol. 55, pp. 1–27. San Diego: Academic Press.
- ASHKIN, A., DZIEDZIC, J., BJORKHOLM, J. & CHU, S. (1986). Observation of a single-beam gradient force optical trap for dielectric particles. *Optical Letters* **11**, 288–290.
- BAI, L., SANTANGELO, T. & WANG, M. (2006). Single-molecule analysis of RNA polymerase transcription. *Annual Review of Biophysics & Biomolecular Structure* **35**, 343–360.
- BAUMANN, C., BLOOMFIELD, V., SMITH, S., BUSTAMANTE, C., WANG, M. & BLOCK, S. (2000). Stretching of single collapsed DNA molecules. *Biophysical Journal* **78**, 1965–1978.
- BELL, G. (1978). Models for the specific adhesion of cells to cells. *Science* **200**, 618–627.
- BONIN, M., ZHU, R., KLAUE, Y., OBERSTRASS, J., OESTERSCHULZE, E. & NELLEN, W. (2002). Analysis of RNA flexibility by scanning force spectroscopy. *Nucleic Acids Research* **30**, 81.
- BRAU, R., TARSA, P., FERRER, J., LEE, P. & LANG, M. (2006). Interlaced optical force-fluorescence measurements for single molecule biophysics. *Biophysical Journal* **91**, 1069–1077.
- BUSTAMANTE, C., MARKO, J., STIGGIA, E. & SMITH, S. (1994). Entropic elasticity of lambda-phage DNA. *Science* **265**, 1599–1600.
- CLAUSEN-SCHAUMANN, H., SEITZ, M., KRAUTBAUER, R. & GAUB, H. (2000). Force spectroscopy with single biomolecules. *Current Opinion in Chemical Biology* **4**, 524–530.
- COCCO, S., MARKO, J. & MONASSON, R. (2003a). Slow nucleic acid unzipping kinetics from sequence-defined barriers. *European Physical Journal E* **10**, 153–161.
- COCCO, S., MARKO, J., MONASSON, R., SARKAR, A. & YAN, J. (2003b). Force-extension behavior of folding polymers. *European Physical Journal E* **10**, 249–263.
- COLLIN, D., RITORT, F., JARZYNSKI, C., SMITH, S., TINOCO, I. J. & BUSTAMANTE, C. (2005). Verification of the Crooks fluctuation theorem and recovery of RNA folding free energies. *Nature* **437**, 231–234.
- CRISONA, N., STRICK, T., BENSIMON, D., CROQUETTE, V. & COZZARELLI, N. (2000). Preferential relaxation of positively supercoiled DNA by E. coli topoisomerase IV in single-molecule and ensemble measurements. *Genes & Development* **14**, 2881–2892.
- CROOKS, G. (1999). Entropy production fluctuation theorem and the nonequilibrium work relation for free-energy differences. *Physical Review E* **60**, 2721–2726.
- CUI, S., ALBRECHT, C., KUHNER, F. & GAUB, H. (2006). Weakly bound water molecules shorten single-stranded DNA. *Journal of the American Chemical Society* **128**, 6636–6639.
- DESSINGES, M., LIONNET, T., XI, X., BENSIMON, D. & CROQUETTE, V. (2004). Single-molecule assay reveals strand switching and enhanced processivity of UvrD. *Proceedings of the National Academy of Sciences USA* **101**, 6439–6444.
- DUMONT, S., WEI, C., SEREBROV, V., BERAN, R., TINOCO, I. J., PYLE, A. & BUSTAMANTE, C. (2006). RNA translocation and unwinding mechanism of HCV NS3 helicase and its coordination by ATP. *Nature* **439**, 105–108.
- EVANS, E. & RITCHIE, K. (1997). Dynamic strength of molecular adhesion bonds. *Biophysical Journal* **72**, 1541–1555.
- FERNANDEZ, J. M. & LI, H. (2004). Force-clamp spectroscopy monitors the folding trajectory of a single protein. *Science* **303**, 1674–1678.
- FLORY, P. J. (1969). *Statistical Mechanics of Chain Molecules*, Appendix G. New York: Interscience Publishers.
- GITTES, F. & SCHMIDT, C. (1998). Signal and noise in micromechanical measurements. *Methods in Cell Biology* **55**, 129–171.
- GORE, J., BRYANT, Z., STONE, M., NÖLLMANN, M., COZZARELLI, N. & BUSTAMANTE, C. (2006). Mechanochemical analysis of DNA gyrase using rotor bead tracking. *Nature* **439**, 100–104.
- GOSSE, C. & CROQUETTE, V. (2002). Magnetic tweezers: micromanipulation and force measurement at the molecular level. *Biophysical Journal* **82**, 3314–3329.
- GREEN, N., WILLIAMS, P., WAHAB, O., DAVIES, M., ROBERTS, C., TENDLER, S. & ALLEN, S. (2004). Single-molecule investigation of RNA dissociation. *Biophysical Journal* **86**, 3811–3821.
- GREENLEAF, W., WOODSIDE, M., ABBONDANZIERI, E. & BLOCK, S. (2005). Passive all-optical force clamp for high-resolution laser trapping. *Physical Review Letters* **95**, 208102.
- GROSS, S. (2003). Application of optical traps in vivo. *Methods in Enzymology* **361**, 162–174.
- GUTOWSKY, H. & HOLM, H. (1957). Rate processes and nuclear magnetic resonance spectra. II. Hindered internal rotation of amides. *Journal of Chemical Physics* **25**, 1228–1234.
- HUGEL, T., HOLLAND, N., CATTANI, A., MORODER, L., SEITZ, M. & GAUB, H. (2002). Single-molecule optomechanical cycle. *Science* **296**, 1103–1106.

- HUMMER, G. & SZABO, A. (2001). Free-energy reconstruction from nonequilibrium single molecule experiments. *Proceedings of the National Academy of Sciences USA* **98**, 3658–3661.
- HYEON, C. & THIRUMALAI, D. (2005). Mechanical unfolding of RNA hairpins. *Proceedings of the National Academy of Sciences USA* **102**, 6789–6794.
- HYEON, C. & THIRUMALAI, D. (2006). Force-unfolding and force-quench refolding of RNA hairpins. *Biophysical Journal* **90**, 3410–3427.
- JACKS, T. & VARMA, H. (1985). Expression of the Rous sarcoma virus *pol* gene by ribosomal frameshifting. *Science* **230**, 1237–1242.
- JARZYNSKI, C. (1997). Nonequilibrium equality for free energy differences. *Physical Review Letters* **78**, 2690–2693.
- JERNIGAN, R. & FLORY, P. (1968). Moments of chain vectors for models of polymer chains. *Journal of Chemical Physics* **50**, 4178–4185.
- KELLER, D., SWIGON, D. & BUSTAMANTE, C. (2003). Relating single-molecule measurements to thermodynamics. *Biophysical Journal* **84**, 733–738.
- LANG, M., ASBURY, C., SHAEVITZ, J. & BLOCK, S. (2002). An automated two-dimensional optical force clamp for single molecule studies. *Biophysical Journal* **83**, 491–501.
- LANG, M. & BLOCK, S. (2002). Resource letter: LBOT-1: laser-based optical tweezers. *American Journal of Physics* **71**, 201–215.
- LANG, M., FORDYCE, P., ENGH, A., NEUMAN, K. & BLOCK, S. (2004). Simultaneous, coincident optical trapping and single-molecule fluorescence. *Nature Methods* **1**, 133–139.
- LECKBAND, D. (1995). The surface apparatus – a tool for probing molecular protein interactions. *Nature* **376**, 617–618.
- LI, P., COLLIN, D., SMITH, S., BUSTAMANTE, C. & TINOCO, I. J. (2006). Probing the mechanical folding kinetics of TAR RNA by hopping, force-jump, and force-ramp methods. *Biophysical Journal* **90**, 250–260.
- LIPHARDT, J., DUMONT, S., SMITH, S., TINOCO, I. J. & BUSTAMANTE, C. (2002). Equilibrium information from nonequilibrium measurements in an experimental test of Jarzynski's equality. *Science* **296**, 1832–1835.
- LIPHARDT, J., ONOA, B., SMITH, S., TINOCO, I. J. & BUSTAMANTE, C. (2001). Reversible unfolding of single RNA molecules by mechanical force. *Science* **292**, 733–737.
- MANOSAS, M. & RITORT, F. (2005). Thermodynamic and kinetic aspects of RNA pulling experiments. *Biophysical Journal* **88**, 3224–3242.
- MAO, H., ARIAS-GONZALEZ, J., SMITH, S., TINOCO, I. J. & BUSTAMANTE, C. (2005). Temperature control methods in a laser tweezers system. *Biophysical Journal* **89**, 1308–1316.
- MARSZALEK, P., LI, H., OBERHAUSER, A. & FERNANDEZ, J. (2002). Chair-boat transitions in single polysaccharide molecules observed with force-ramp AFM. *Proceedings of the National Academy of Sciences USA* **99**, 4278–4283.
- MATHEWS, D., DISNEY, M., CHILDS, J., SCHROEDER, S., ZUKER, M. & TURNER, D. (2004). Incorporating chemical modification constraints into a dynamic programming algorithm for prediction of RNA secondary structure. *Proceedings of the National Academy of Sciences USA* **101**, 7287–7292.
- MATHEWS, D., SABINA, J., ZUKER, M. & TURNER, D. (1999). Expanded sequence dependence of thermodynamic parameters improves prediction of RNA secondary structure. *Journal of Molecular Biology* **288**, 911–940.
- NAMY, O., MORAN, S., STUART, D., GILBERT, R. & BRIERLEY, I. (2006). A mechanical explanation of RNA pseudoknot function in programmed ribosomal frameshifting. *Nature* **441**, 244–247.
- NEUMAN, K. & BLOCK, S. (2004). Optical trapping. *Review of Scientific Instruments* **75**, 2787–2809.
- ONOA, B., DUMONT, S., LIPHARDT, J., SMITH, S., TINOCO, I. J. & BUSTAMANTE, C. (2003). Identifying kinetic barriers to mechanical unfolding of the *T. thermophila* ribozyme. *Science* **299**, 1892–1895.
- PLANT, E., JACOBS, K., HARGER, J., MESKAUSKAS, A., JACOBS, J., BAXTER, J., PETROV, A. & DINMAN, J. (2003). The 9-A solution: how mRNA pseudoknots promote efficient programmed -1 ribosomal frameshifting. *RNA* **9**, 168–174.
- REVVYAKIN, A., ALLEMAND, J., CROQUETTE, V., EBRIGHT, R. & STRICK, T. (2003). Single-molecule DNA nanomanipulation: detection of promoter-unwinding events by RNA polymerase. *Methods in Enzymology* **370**, 577–598.
- RIEF, M., CLAUSEN-SCHAUMANN, H. & GAUB, H. (1999). Sequence-dependent mechanics of single DNA molecules. *Nature Structural Biology* **6**, 346–349.
- RIEF, M., GAUTEL, M., OESTERHELT, F., FERNANDEZ, J. M. & GAUB, H. E. (1997). Reversible unfolding of individual titin immunoglobulin domains by AFM. *Science* **276**, 1109–1112.
- RITORT, F., BUSTAMANTE, C. & TINOCO, I. J. (2002). A two-state kinetic model for the unfolding of single molecules by mechanical force. *Proceedings of the National Academy of Sciences USA* **99**, 13544–13548.
- ROSA, A., HOANG, T., MARENDUZZO, D. & MARITAN, A. (2005). A new interpolation formula for semiflexible polymers. *Biophysical Chemistry* **115**, 251–254.
- SEOL, Y., SKINNER, G. & VISSCHER, K. (2004). Elastic properties of a single-stranded charged homopolymeric ribonucleotide. *Physical Review Letters* **93**, 118102.
- SHEETZ, M. (1998). Laser tweezers in cell biology. In *Methods in Cell Biology*, vol. 55. San Diego: Academic Press.
- SMITH, S., CUI, Y. & BUSTAMANTE, C. (1996). Overstretching B-DNA: the elastic response of individual double-stranded and single-stranded DNA molecules. *Science* **271**, 795–799.

- SMITH, S., CUI, Y. & BUSTAMANTE, C. (2003). Optical-trap force transducer that operates by direct measurement of light momentum. *Methods in Enzymology* **361**, 134–162.
- STEINFELD, J., FRANCISCO, J. & HASE, W. (1989). *Chemical Kinetics and Dynamics*. Englewood Cliffs, NJ: Prentice Hall.
- STRICK, T., ALLEMAND, J., BENSIMON, D., BENSIMON, A. & CROQUETTE, V. (1996). The elasticity of a single supercoiled DNA molecule. *Science* **271**, 1835–1837.
- SVOBODA, K. & BLOCK, S. (1994). Biological applications of optical forces. *Annual Review of Biophysics & Biomolecular Structure* **23**, 247–285.
- TINOCO, I. J. (2004). Force as a useful variable in reactions: unfolding RNA. *Annual Review of Biophysics & Biomolecular Structure* **33**, 363–385.
- TINOCO, I. J., UHLENBECK, O. & LEVIN, M. (1971). Estimation of secondary structure in ribonucleic acids. *Nature* **230**, 362–367.
- VIEREGG, J. & TINOCO, I. J. (2006). Modeling RNA folding under mechanical tension. *Molecular Physics* **104**, 1343–1352.
- WIGGINS, P., PHILLIPS, R. & NELSON, P. (2005). Exact theory of kinkable elastic polymers. *Physical Review E* **71**, 021909.
- WILLIAMS, M., WENNER, J., ROUZINA, I. & BLOOMFIELD, V. (2001). Entropy and heat capacity of DNA melting from temperature dependence of single molecule stretching. *Biophysical Journal* **80**, 1932–1939.
- WOODSIDE, M., BEHNKE-PARKS, W., LARIZADEH, K., TRAVERS, K., HERSCHLAG, D. & BLOCK, S. (2006). Nanomechanical measurements of the sequence-dependent folding landscapes of single nucleic acid hairpins. *Proceedings of the National Academy of Sciences USA* **103**, 6190–6195.
- ZUKER, M. (2003). Mfold web server for nucleic acid folding and hybridization prediction. *Nucleic Acids Research* **31**, 3406–3415.